











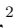






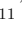

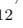










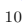
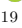










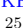
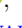



























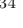


UVCANDELS: Catalogs of photometric redshifts and galaxy physical properties

VIHANG MEHTA ¹, MARC RAFELSKI ^{2,3}, BEN SUNNQUIST ², HARRY I. TEPLITZ ¹, CLAUDIA SCARLATA ⁴,
XIN WANG ^{5,6}, ADRIANO FONTANA ⁷, NIMISH P. HATHI ², KARTHEIK G. IYER ⁸, ANAHITA ALAVI ¹,
JAMES COLBERT ¹, NORMAN GROGIN ², ANTON KOEKEMOER ², KALINA V. NEDKOVA ^{3,2}, MATTHEW HAYES ⁹,
LAURA PRICHARD ², BRIAN SIANA ¹⁰, BRENT M. SMITH ¹¹, ROGIER WINDHORST ¹¹, TERESA ASHCRAFT ¹¹,
MICAELA BAGLEY ¹², IVANO BARONCHELLI ¹³, GUILLERMO BARRO ¹⁴, ALEX BLANCHE ¹¹, ADAM BROUSSARD ¹⁵,
TIMOTHY CARLETON ¹¹, NIMA CHARTAB ¹⁶, ALEX CODOREANU ¹⁷, SETH COHEN ¹¹, CHRISTOPHER CONSELICE ¹⁸,
Y. SOPHIA DAI ⁶, BEHNAM DARVISH ¹⁰, ROMEEEL DAVÉ ¹⁹, LAURA DEGROOT ²⁰, DUILIA DE MELLO ²¹,
MARK DICKINSON ²², NAJMEH EMAMI ¹⁰, HENRY FERGUSON ², LEONARDO FERREIRA ²³, KEELY FINKELSTEIN ¹²,
STEVEN FINKELSTEIN ¹², JONATHAN P. GARDNER ²⁴, ERIC GAWISER ¹⁵, TIMOTHY GBUREK ¹⁰,
MAURO GIAVALISCO ²⁵, ANDREA GRAZIAN ¹³, CARYL GRONWALL ²⁶, YICHENG GUO ²⁷, PABLO ARRABAL HARO ²²,
SHOUBANEH HEMMATI ¹, JUSTIN HOWELL ¹, ROLF A. JANSEN ¹¹, ZHIYUAN JI ²⁵, SUGATA KAVIRAJ ²⁸,
KEUNHO J. KIM ¹, PETER KURCZYNSKI ²⁴, ILIN LAZAR ²⁹, RAY A. LUCAS ², JOHN MACKENY ²,
KAMESWARA BHARADWAJ MANTHA ⁴, ALEC MARTIN ²⁷, GARRETH MARTIN ^{30,31}, TYLER MCCABE ¹¹,
BAHRAM MOBASHER ¹⁰, ALEXA M. MORALES ¹², ROBERT O'CONNELL ³², CHARLOTTE OLSEN ¹⁵,
LILLIAN OTTESON ¹¹, SWARA RAVINDRANATH ², CALEB REDSHAW ¹¹, MICHAEL RUTKOWSKI ³³,
BRANT ROBERTSON ³⁴, ZAHRA SATTARI ¹⁰, EMMARIS SOTO ³⁵, LEI SUN ⁵, SINA TAAMOLI ¹⁰, EROS VANZELLA ³⁶,
L. Y. AARON YUNG ², BONNABELLE ZABELLE ⁴ AND THE UVCANDELS TEAM

¹IPAC, Mail Code 314-6, California Institute of Technology, 1200 E. California Blvd., Pasadena, CA, 91125, USA

²Space Telescope Science Institute, 3700 San Martin Drive, Baltimore, MD 21218, USA

³Department of Physics and Astronomy, Johns Hopkins University, Baltimore, MD 21218, USA

⁴Minnesota Institute for Astrophysics, University of Minnesota, 116 Church St SE, Minneapolis, MN 55455, USA

⁵School of Astronomy and Space Science, University of Chinese Academy of Sciences (UCAS), Beijing 100049, China

⁶National Astronomical Observatories, Chinese Academy of Sciences, Beijing 100101, China

⁷INAF – Osservatorio Astronomico di Roma – via Frascati 33, Monte Porzio Catone, 00078 Rome, Italy

⁸Columbia Astrophysics Laboratory, Columbia University, 550 West 120th Street, New York, NY 10027, USA

⁹Stockholm University, Department of Astronomy and Oskar Klein Centre for Cosmoparticle Physics, SE-10691, Stockholm, Sweden

¹⁰Department of Physics and Astronomy, University of California, Riverside, Riverside, CA 92521, USA

¹¹School of Earth and Space Exploration, Arizona State University, Tempe, AZ 85287, USA

¹²Department of Astronomy, The University of Texas at Austin, Austin, TX 78712, USA

¹³INAF – Osservatorio Astronomico di Padova, Vicolo dell'Osservatorio 5, I-35122, Padova, Italy

¹⁴Department of Physics, University of the Pacific, Stockton, CA 95211, USA

¹⁵Department of Physics and Astronomy, Rutgers, The State University of New Jersey, Piscataway, NJ 08854, USA

¹⁶Observatories of the Carnegie Institution of Washington, Pasadena, CA 91101, US

¹⁷Centre for Astrophysics and Supercomputing, Swinburne University of Technology, Hawthorn VIC 3122, Australia

¹⁸School of Physics and Astronomy, The University of Nottingham, University Park, Nottingham NG7 2RD, UK

¹⁹Institute for Astronomy, University of Edinburgh, Edinburgh, EH9 3HJ, UK

²⁰College of Wooster, Wooster, OH 44691, USA

²¹Department of Physics, The Catholic University of America, Washington, DC 20064, USA

²²NSF's NOIRLab, Tucson, AZ 85719, USA

²³Centre for Astronomy and Particle Physics, School of Physics and Astronomy, University of Nottingham, NG7 2RD, UK

²⁴Astrophysics Science Division, NASA Goddard Space Flight Center, Greenbelt, MD 20771, USA

²⁵Department of Astronomy, University of Massachusetts, Amherst, MA 01003, USA

²⁶Department of Astronomy & Astrophysics, The Pennsylvania State University, University Park, PA 16802, USA

²⁷Department of Physics and Astronomy, University of Missouri, Columbia, MO 65211, USA

²⁸Centre for Astrophysics Research, University of Hertfordshire, Hatfield, AL10 9AB, UK

²⁹Department of Galaxies and Cosmology, Max Planck Institute for Astronomy, Königstuhl 17, 69117 Heidelberg

³⁰*Korea Astronomy and Space Science Institute, Yuseong-gu, Daejeon 34055, Korea*

³¹*Steward Observatory, University of Arizona, Tucson, AZ 85719, USA*

³²*Department of Astronomy, University of Virginia, Charlottesville, VA 22904*

³³*Department of Physics and Astronomy, Minnesota State University Mankato, Mankato, MN 56001, USA*

³⁴*Department of Astronomy and Astrophysics, University of California, Santa Cruz, Santa Cruz, CA 95064, USA*

³⁵*Computational Physics, Inc., Springfield, VA 22151, USA*

³⁶*INAF – Osservatorio di Astrofisica e Scienza dello Spazio di Bologna, via Gobetti 93/3, I-40129 Bologna, Italy*

ABSTRACT

The UltraViolet imaging of the Cosmic Assembly Near-infrared Deep Extragalactic Legacy Survey Fields (UVCANDELS) program provides deep *HST* F275W and F435W imaging over four CANDELS fields (GOODS-N, GOODS-S, COSMOS, and EGS). We combine this newly acquired UV imaging with existing *HST* imaging from CANDELS as well as existing ancillary data to obtain robust photometric redshifts and reliable estimates for galaxy physical properties for over 150,000 galaxies in the ~ 430 arcmin² UVCANDELS area. Here, we leverage the power of the new UV photometry to not only improve the photometric redshift measurements in these fields, but also constrain the full redshift probability distribution combining multiple redshift fitting tools. Furthermore, using the full UV-to-IR photometric dataset, we measure the galaxy physical properties by fitting templates from population synthesis models with two different parameterizations (flexible and fixed-form) of the star-formation histories (SFHs). Compared to the flexible SFH parametrization, we find that the fixed-form SFHs systematically underestimate the galaxy stellar masses, both at the low- ($\lesssim 10^9 M_\odot$) and high- ($\gtrsim 10^{10} M_\odot$) mass end, by as much as ~ 0.5 dex. This underestimation is primarily due the limited ability of fixed-form SFH parameterization to simultaneously capture the chaotic nature of star-formation in these galaxies.

Keywords: catalogs — galaxies: redshifts — galaxies: fundamental parameters — methods: observational — techniques: photometric

1. INTRODUCTION

Over the past few decades, our knowledge of galaxy formation and evolution has seen significant advancement and large multi-wavelength photometric surveys have been one of the cornerstones enabling this progress. Space-based facilities such as *HST*, *Spitzer*, and now *JWST* have granted access not only to high-resolution and extremely sensitive imaging, but also to wavelengths that are otherwise inaccessible from the ground. The combination of space- and ground-based observations covering wavelengths from the far ultraviolet (UV) out to mid-infrared (IR) have facilitated detailed studies of galaxies and the physical processes that govern how they grow and evolve over time – namely, tracing the evolution of the stellar mass function over time (e.g., Marchesini et al. 2009; Muzzin et al. 2013; Davidzon et al. 2017; Weaver et al. 2023; Weibel et al. 2024), the cosmic star-formation rate and its evolution (e.g., Madau & Dickinson 2014; Alavi et al. 2014, 2016; Mehta et al. 2017; Moutard et al. 2020; Picouet et al. 2023), the star-forming main sequence (e.g., Speagle et al. 2014; Whitaker et al. 2014; Kurczynski et al. 2016; Boogaard et al. 2018; Mérida et al. 2023), and the mass-size re-

lation (e.g., Shen et al. 2003; Baldry et al. 2012; Morishita et al. 2017; Nedkova et al. 2021, 2024), among others. Particularly, the WFC3/UVIS instrument on-board *HST* has been monumental by providing access to the rest-frame UV light from galaxies which is key for studying their star-formation properties and hence, tracking their growth as well as for constraining the amount of dust in them.

One such pivotal photometric survey has been the Cosmic Assembly Near-Infrared Deep Extragalactic Legacy Survey (CANDELS; Grogin et al. 2011; Koekoemoer et al. 2011), which is a legacy *HST* program that obtained WFC3/IR and ACS/WFC optical imaging in up to 10 broadband filters for five extragalactic fields (GOODS-N, GOODS-S, COSMOS, EGS, and UDS) over a combined area of ~ 0.2 deg². Complemented with additional observations with *Spitzer* and various other ground-based instruments, the CANDELS fields serve as one of the premier observational datasets for studying galaxy evolution and have already enabled a wide range of science. The CANDELS team has previously assembled catalogs that include multi-wavelength photometric coverage for the *HST* as well as all ancillary

data available on these fields (Guo et al. 2013; Nayyeri et al. 2017; Stefanon et al. 2017; Barro et al. 2019).

Recently, another *HST* Treasury campaign, UVCANDELS (PI: H. Teplitz; PID: 15647; Wang et al. 2024), accomplished the task of obtaining UV imaging with F275W and F435W (in parallel) over four of the five CANDELS fields (GOODS-N, GOODS-S, COSMOS, EGS). The new F435W coverage in COSMOS and EGS fields overlaps with that of F275W which previously did not have F435W; while in GOODS-N and GOODS-S, the parallel F435W coverage is limited to the deeper regions (not overlapping with F275W) given the existing F435W data already available for the UVCANDELS regions. The additional UV coverage improves the photometric redshift estimates, particularly for objects that have degenerate solutions, typically characterized as multiple peaks in their photometric redshift probability distributions that are significant (e.g., $\gtrsim 10\%$ of the primary peak) and sufficiently separated in redshift (e.g., $\Delta z/(1+z) \gtrsim 0.06$), which when not appropriately accounted for can lead to catastrophic errors in the measured redshifts and associated uncertainties (e.g., Rafelski et al. 2009, 2015). The UV imaging helps prevent this for example by sampling the Lyman break of $z \sim 2$ galaxies removing the degeneracy with the Balmer break of $z \sim 0.3$ galaxies. Similarly, the UV photometry is critical to accurately constrain the recent star-formation activity and dust content of galaxies (e.g., Mehta et al. 2017, 2023). In this work, we leverage the existing multi-wavelength CANDELS photometry with the addition of the new F275W and F435W photometry from UVCANDELS to provide improved photometric redshifts as well as galaxy physical properties for over 150,000 galaxies in these four CANDELS fields.

Estimating both photometric redshifts and physical parameters via modeling the galaxy spectral energy distribution (SED) has been well established with a vast library of tools with varying levels of sophistication now available for both (e.g., Rafelski et al. 2015; Mehta et al. 2018; Kodra et al. 2023; Pacifici et al. 2023). However, variations in template choices and codes result in slightly different results (e.g., Dahlen et al. 2013). In this work, we leverage the power of multiple photometric redshift fitting tools and template sets and combine their results to yield robust redshift estimates as well as to accurately quantify the redshift probability distributions. When estimating the galaxy physical properties, the star-formation history (SFH) plays an essential role in determining the galaxy SED (e.g., Iyer et al. 2019; Leja et al. 2019) and traditionally, SFHs in typical SED fitting tools have been assumed to have a fixed,

functional forms. However, there is increasing evidence suggesting that galaxy SFHs, particularly in the early universe as well as toward the low-mass end, are not smoothly evolving, rather they are chaotic and often bursty in nature, both from a theoretical (see e.g., Hopkins et al. 2014; Domínguez et al. 2015; Sun et al. 2023a) as well as observational perspectives (see e.g. Weisz et al. 2012; Emami et al. 2019; Mehta et al. 2017, 2023). In this work, we explore the impact of the traditional fixed-form SFH assumption for even the most basic physical parameter – i.e., galaxy stellar mass – by comparing to results from fitting tools that accommodate more flexible forms for the galaxy SFH.

This manuscript is organized as follows: Section 2 describes the UVCANDELS dataset as well as the ancillary photometric datasets used for this analysis; Section 3 describes the techniques used for estimating photometric redshifts and discusses the improvement in the redshift estimates by the inclusion of the UV photometry; Section 4 describes the methodologies used for the measurements of galaxy physical parameters and discusses the impact of the fixed vs. flexible-form for the galaxy SFHs on the estimated physical parameters; Section 5 describes the final output catalogs that present the various measurements from this work and presents the publicly released catalogs; and Section 6 summarizes our findings.

Throughout this paper, we adopt cosmological parameters from Table 3 of Planck Collaboration et al. (2016): $\Omega_m = 0.315$, $\Omega_\lambda = 0.685$ and $H_0 = 67.31 \text{ km s}^{-1} \text{ Mpc}^{-1}$ and all magnitudes used are AB magnitudes (Oke & Gunn 1983).

2. DATA

2.1. UVCANDELS Imaging

The Ultraviolet Imaging of the Cosmic Assembly Near-infrared Deep Extragalactic Legacy Survey fields (UVCANDELS; PI: H. Teplitz; PID: 15647; Wang et al. 2024) is a Cycle 26 *Hubble* Treasury program that obtained WFC3/UVIS F275W and ACS/WFC F435W (in parallel) for four of the deep-wide survey fields defined by CANDELS (Grogin et al. 2011; Koekemoer et al. 2011), namely GOODS-N, GOODS-S, COSMOS, and EGS, covering a combined area of $\sim 430 \text{ arcmin}^2$. The UVCANDELS imaging reaches a depth of AB=27 for compact galaxies in the WFC3/UVIS F275W filter, and AB \leq 28 in ACS/F435W. The UVCANDELS F275W mosaics are available at the Mikulski Archive for Space Telescopes (MAST; doi:10.17909/8s31-f778)¹

¹ <https://archive.stsci.edu/hlsp/uvcandels>

for all four fields along with F435W mosaics for COSMOS and EGS². These UVCANDELS image mosaics are aligned and registered to the CANDELS astrometry. With the newly acquired UVCANDELS imaging, we have measured the fluxes in the F275W filter for the four fields and F435W for COSMOS and EGS. See Wang et al. (2024) and Sun et al. (2023b) for full details on the methodology to generate the mosaics and photometric catalogs, respectively.

2.2. Photometric Datasets

The photometric dataset used for modeling the galaxy spectral energy distributions (SEDs) in this work are primarily based on the publicly available CANDELS catalogs³, with the addition of the new F275W and F435W UVCANDELS photometry. Specifically, the CANDELS multi-wavelength photometric catalogs that we use for GOODS-N, GOODS-S, COSMOS and EGS fields are described and presented in Barro et al. (2019), Guo et al. (2013), Nayyeri et al. (2017), and Stefanon et al. (2017), respectively. Similarly, the photometric techniques used for measuring the F275W and F435W fluxes as well as the catalogs from UVCANDELS are fully described in detail in Sun et al. (2023b). These F275W and F435W fluxes from UVCANDELS are measured in a consistent fashion as the rest of the CANDELS photometry (see Section 2.3 for more details). For completeness, we briefly summarize the various surveys that make up the full photometric dataset for each field in the subsections below as well as in Table 1.

2.2.1. GOODS-N

We use the photometric catalog from Barro et al. (2019) for the GOODS-N field (Giavalisco et al. 2004). For the SED modeling, we consider the photometry for *HST*/ACS optical imaging in F435W, F606W, F775W, F814W, and F850LP from the GOODS *HST*/ACS Treasury Program (Giavalisco et al. 2004), the CANDELS survey (Grogin et al. 2011; Koekemoer et al. 2011), as well as the search for high-redshift Type Ia supernovae (e.g., Riess et al. 2007). We include photometry for *HST*/WFC3 imaging in the NIR filters F105W, F125W, and F160W from the CANDELS survey as well as additional F140W coverage from the G141 AGHAST survey (Weiner 2009). We further include the new *HST*/WFC3

F275W photometry available from the UVCANDELS imaging (Wang et al. 2024; Sun et al. 2023b).

In addition to the *HST* imaging, we also use the ground-based *LBT*/LBC *U'*-band photometry from Grazian et al. (2017) as well as the K_s -band photometry from *Subaru*/MOIRCS (Kajisawa et al. 2011) and *CFHT*/WIRCam (Hsu et al. 2019). Lastly, we include *Spitzer*/IRAC ch. 1 (3.6 μm), 2 (4.5 μm), 3 (5.8 μm), 4 (8.0 μm) photometry available from a combination of the *Spitzer* Extended Deep Survey (SEDS, Ashby et al. 2013), the *Spitzer*-CANDELS (S-CANDELS, Ashby et al. 2015), and *Spitzer*-GOODS (Dickinson et al. 2003) surveys.

2.2.2. GOODS-S

Guo et al. (2013) present in full detail the photometric catalog that we use for the GOODS-S field. Similar to GOODS-N, the photometry for *HST*/ACS F435W, F606W, F775W, F814W, and F850LP is provided from the GOODS *HST*/ACS Treasury Program, the CANDELS survey, as well as the search for high-redshift Type Ia supernovae. The *HST*/WFC3 photometry for F098M, F105W, F125W, and F160W is provided from the CANDELS, HUDF (Bouwens et al. 2010), and ERS (Windhorst et al. 2011) programs. Critically, we add the new *HST*/WFC3 F275W photometry from UVCANDELS (Wang et al. 2024; Sun et al. 2023b).

Furthermore, photometry from ground-based imaging in the U-band from *Blanco*/MOSAIC II and *VLT*/VIMOS (Nonino et al. 2009) is included as well as the K_s -band from *VLT*/ISAAC (Retzlaff et al. 2010) and *VLT*/HAWK I (Fontana et al. 2014). Lastly, *Spitzer*/IRAC ch. 1, 2, 3, 4 photometry available from a combination of SEDS (Ashby et al. 2013), and the *Spitzer*-GOODS (Dickinson et al. 2003) survey is also included.

2.2.3. COSMOS

For the COSMOS field (Scoville et al. 2007), we utilize the catalog from Nayyeri et al. (2017) for all photometry except for *HST*/WFC3 F275W and *HST*/ACS F435W which are provided from UVCANDELS (Wang et al. 2024; Sun et al. 2023b). We include the photometry in *HST*/ACS imaging filters F606W, F814W as well as in *HST*/WFC3 NIR filters F125W, F140W from the CANDELS survey.

There exists a wealth of ancillary ground-based data for the COSMOS field. Here, we include the photometry from *CFHT*-LS *ugriz*-bands (Gwyn 2012), *Subaru*/Suprime-Cam $Bg^+Vr^+i^+z^+$ from Taniguchi et al. (2015), and *VISTA*/VIRCAM $YJHK_s$ from the UltraVISTA survey (McCracken et al. 2012). We also include the medium-band photometry from the NEW-

² The F435W mosaics for GOODS-N and GOODS-S covered by UVCANDELS are already available from CANDELS.

³ <https://archive.stsci.edu/hlsp/candels>

Table 1. The set of photometric filters included for SED modeling, both when measuring the photometric redshifts as well as the galaxy physical parameters

Field	Instrument	Filter	Survey/Reference
GOODS-N ^a	<i>HST</i> /UVIS	F275W ^b	UVCANDELS (Wang et al. 2024; Sun et al. 2023b)
	<i>HST</i> /ACS	F435W, F606W, F775W, F814W, F850LP	GOODS (Giavalisco et al. 2004), CANDELS (Grogin et al. 2011; Koekemoer et al. 2011), Riess et al. (2007)
	<i>HST</i> /WFC3	F105W, F125W, F140W, F160W	CANDELS (Grogin et al. 2011; Koekemoer et al. 2011), AGHAST (Weiner 2009)
	<i>LBT</i> /LBC	<i>U'</i>	Grazian et al. (2017)
	<i>Subaru</i> /MOIRCS	<i>K_s</i>	Kajisawa et al. (2011)
	<i>CFHT</i> /WIRCam	<i>K_s</i>	Hsu et al. (2019)
	<i>Spitzer</i> /IRAC	ch. 1, 2, 3, 4	SEDS (Ashby et al. 2013), S-CANDELS (Ashby et al. 2015), Spitzer-GOODS (Dickinson et al. 2003)
GOODS-S ^a	<i>HST</i> /UVIS	F275W ^b	UVCANDELS (Wang et al. 2024; Sun et al. 2023b)
	<i>HST</i> /ACS	F435W, F606W, F775W, F814W, F850LP	GOODS (Giavalisco et al. 2004), CANDELS (Grogin et al. 2011; Koekemoer et al. 2011), Riess et al. (2007)
	<i>HST</i> /WFC3	F098M, F105W, F125W, F160W	CANDELS (Grogin et al. 2011; Koekemoer et al. 2011), HUDF (Bouwens et al. 2010), ERS (Windhorst et al. 2011)
	<i>Blanco</i> /MOSAIC II	<i>U</i>	Guo et al. (2013)
	<i>VLT</i> /VIMOS	<i>U</i>	Nonino et al. (2009)
	<i>VLT</i> /ISAAC	<i>K_s</i>	Retzlaff et al. (2010)
	<i>VLT</i> /HAWK-I	<i>K_s</i>	Fontana et al. (2014)
<i>Spitzer</i> /IRAC	ch. 1, 2, 3, 4	SEDS (Ashby et al. 2013), Spitzer-GOODS (Dickinson et al. 2003)	
COSMOS ^a	<i>HST</i> /UVIS	F275W ^b	UVCANDELS (Wang et al. 2024; Sun et al. 2023b)
	<i>HST</i> /ACS	F435W ^b , F606W, F814W	UVCANDELS (Wang et al. 2024; Sun et al. 2023b), CANDELS (Grogin et al. 2011; Koekemoer et al. 2011)
	<i>HST</i> /WFC3	F125W, F160W	CANDELS (Grogin et al. 2011; Koekemoer et al. 2011)
	<i>CFHT</i> /MegaPrime	<i>ugriz</i>	CHFT-LS (Gwyn 2012)
	<i>Subaru</i> /Suprime-Cam	<i>Bg⁺Vr⁺i⁺z⁺</i>	Taniguchi et al. (2007, 2015)
	<i>VISTA</i> /VIRCAM	<i>YJHK_s</i>	UltraVISTA (McCracken et al. 2012)
	<i>Mayall</i> /NEWFIRM	<i>J1, J2, J3, H1, H2, K</i>	NMBS (Whitaker et al. 2011)
<i>Spitzer</i> /IRAC	ch. 1, 2, 3, 4	SEDS (Ashby et al. 2013), S-COSMOS (Sanders et al. 2007)	
EGS ^a	<i>HST</i> /UVIS	F275W ^b	UVCANDELS (Wang et al. 2024; Sun et al. 2023b)
	<i>HST</i> /ACS	F435W ^b , F606W, F814W	UVCANDELS (Wang et al. 2024; Sun et al. 2023b), CANDELS (Grogin et al. 2011; Koekemoer et al. 2011)
	<i>HST</i> /WFC3	F125W, F140W, F160W	CANDELS (Grogin et al. 2011; Koekemoer et al. 2011), 3D-HST (Brammer et al. 2012; Skelton et al. 2014)
	<i>CFHT</i> /MegaCam	<i>ugriz</i>	CFHT-LS (Gwyn 2012)
	<i>CFHT</i> /WIRCam	<i>JHK_s</i>	WIRDS (Bielby et al. 2012)
	<i>Mayall</i> /NEWFIRM	<i>J1 J2 J3 H1 H2 K</i>	NMBS (Whitaker et al. 2011)
	<i>Spitzer</i> /IRAC	ch. 1, 2, 3, 4	SEDS (Ashby et al. 2013), S-CANDELS (Ashby et al. 2015), AEGIS (Barmby et al. 2008)

^a All photometry except for that provided by UVCANDELS is from the publicly available CANDELS multi-wavelength photometric catalogs – i.e., Barro et al. (2019) for GOODS-N; Guo et al. (2013) for GOODS-S; Nayyeri et al. (2017) for COSMOS; Stefanon et al. (2017) for EGS.

^b Photometry for the F275W (all four fields) and F435W (COSMOS and EGS) bands is the new addition from UVCANDELS (Wang et al. 2024; Sun et al. 2023b).

FIRM Medium Band Survey (NMBS, Whitaker et al. 2011) for *Mayall*/NEWFIRM $J_1, J_2, J_3, H_1, H_2, K$ -bands. Lastly, the *Spitzer*/IRAC ch. 1, 2, 3, 4 photometry from the S-COSMOS survey (Sanders et al. 2007) is also used.

2.2.4. EGS

The catalog from Stefanon et al. (2017) is used for all photometry in the EGS field except for *HST*/WFC3 F275W and *HST*/ACS F435W filters which are provided from the UVCANDELS imaging (Wang et al. 2024; Sun et al. 2023b). We include the photometry for *HST*/ACS F606W and F814W imaging taken as part of the AEGIS project and the CANDELS survey. The *HST*/WFC3 photometry available in the NIR filters F125W, F140W, and F160W is contributed from a combination of the CANDELS and the 3D-HST Brammer et al. (2012) surveys.

Additionally, photometry from ground-based imaging in *ugriz* from CFHT-LS (Gwyn 2012) is also included along side *CFHT*/WIRCam JHK_s imaging from the WIRCam Deep Survey (WIRDS, Bielby et al. 2012). Similar to COSMOS, we include the medium-band imaging in the *Mayall*/NEWFIRM $J_1, J_2, J_3, H_1, H_2, K$ -bands from NMBS (Whitaker et al. 2011). Lastly, we include the *Spitzer*/IRAC ch. 1, 2, 3, 4 photometry from the SEDS (Ashby et al. 2013), S-CANDELS (Ashby et al. 2015), and AEGIS (Barmby et al. 2008).

2.3. Photometric Measurements

While we refer the reader to the respective publications for the exact details of the photometric techniques used to assemble the multi-wavelength catalogs, we briefly summarize the pertinent details here. For all the CANDELS catalogs considered here, the object detection is performed on the F160W-band image. The isophotes defined on the F160W image are then used to measure the photometry in the remaining bands. For the high-resolution data (i.e., all HST bands), the point-spread function (PSF) for each image is convolved to match the F160W resolution, which has the broadest PSF amongst the HST filters. For the low-resolution images (i.e., ground-based and *Spitzer*/IRAC), the photometry was performed using the TFIT software (Laidler et al. 2007), which uses a morphological template-fitting technique.

For the F275W/F435W photometry added from the UVCANDELS imaging (Wang et al. 2024; Sun et al. 2023b), the F275W and F435W magnitudes are computed using UV-optimized isophotes following the methodology from the Hubble Ultra-Deep Field (UVUDF, Teplitz et al. 2013) UV analysis from Rafelski

et al. (2015). Specifically, instead of following the typical approach of performing PSF-matched photometry using the isophotes defined on images with the broadest PSF (typically F160W for HST imaging data), we use isophotes defined on the F606W image instead to measure the fluxes from the unconvolved F275W/F435W images (without matching PSF), followed by applying an adjustment factor to correct for the aperture and PSF differences to match back to the F160W isophote-based photometry. This has the advantage of having isophotes/apertures that are more appropriately matched to the detected UV sizes, and thus return significantly better signal-to-noise ratio (SNR) for the measured fluxes. In order to keep the photometry consistent with the rest from CANDELS, these F606W-defined isophotes are matched and reconciled back to the F160W-isophotes used by the CANDELS photometric catalogs. This is described as the photometry from the "VtoH" segmentation maps in Sun et al. (2023b), which also provides the full detailed description of this photometric technique and methodology.

For the SED modeling presented in this work, we use the photometry from a combination of the above-described CANDELS and UVCANDELS catalogs. Before proceeding with the fitting, we correct the photometry for galactic extinction using the Schlegel et al. (1998) dust maps⁴. The reddening $E(B - V)$ is queried at the position of each galaxy and converted to an extinction assuming a Cardelli et al. (1989) extinction law, for the respective filters.

3. PHOTOMETRIC REDSHIFTS

There are many different photometric redshift codes available, and they all yield slightly different results when run on the same data (e.g. Dahlen et al. 2013; Kodra et al. 2023). In this work, we opt to utilize multiple codes and combine the results, which yields more robust redshifts than any individual code due to different systematic uncertainties in the codes and choice of template spectra. Specifically, we calculate photometric redshifts by combining the results from four different codes: EAZY (Brammer et al. 2008), BPZ (Coe et al. 2006), LEPHARE (Arnouts et al. 1999; Ilbert et al. 2006), and ZPHOT (Giallongo et al. 1998; Fontana et al. 2000). These codes were chosen as they were consistently among the top performers in photometric redshift review papers of CANDELS fields (Hildebrandt et al. 2010; Dahlen et al. 2013).

⁴ Specifically, we use the Python implementation from <https://github.com/adrn/SFD> to query the Schlegel et al. (1998) maps.

We run two separate iterations of EAZY (Brammer et al. 2008) to give us a total of 5 independent code run results. The first EAZY iteration uses the default template spectra (`eazy_v1.2_dusty`) which includes the 6 original templates from Brammer et al. (2008), emission lines from Ilbert et al. (2009), an old and red SED from Maraston (2005), and a dusty SED from Bruzual & Charlot (2003). The second EAZY iteration uses the five templates from Blanton & Roweis (2007) (`br07_default`). Both template sets use a non-negative matrix factorization to optimally select a reduced set of spectral templates that reproduce observed data (Blanton & Roweis 2007). The first template set is optimized for high redshift galaxies from theoretical models, while the second is optimized for lower redshifts based on empirical SDSS data. For both iterations, EAZY is restricted to a redshift range 0 to 12.

For BPZ (Benítez 2000; Benítez et al. 2004; Coe et al. 2006), we use the improved software and procedure described in Rafelski et al. (2015), which includes 11 template SEDs based on those from PEGASE (Fioc & Rocca-Volmerange 1997) but re-calibrated based on photometric and spectroscopic redshifts from FIREWORKS (Wuyts et al. 2008), and a prior based on luminosity functions observed in COSMOS (Ilbert et al. 2009), GOODS-MUSIC (Grazian et al. 2006; Santini et al. 2009), and the UDF (Coe et al. 2006).

The other two codes were used with their default template sets. For LEPHARE (Arnouts et al. 1999; Ilbert et al. 2006), we use the 32 COSMOS SEDs described in Ilbert et al. (2009), and correct for emission lines and extinction using the reddening laws from Calzetti et al. (2000) and Prevot et al. (1984). For ZPHOT (Giallongo et al. 1998; Fontana et al. 2000), we use SED templates from Bruzual & Charlot (2003) with the addition of Calzetti et al. (2000) extinction and Fan et al. (2006) absorption due to the inter-galactic medium (IGM).

We note that sometimes photometric redshifts are calculated iteratively, implementing zero-point offsets to the photometry or modifying the templates based on the spectroscopic redshifts (e.g. Barro et al. 2019). This can often improve the photometric redshift accuracy, although a number of the templates used in this study are already optimized based on empirical data. We found that, on average, the dispersion of the redshifts were improved by modifying the zero-points, but that it worsened the results at $z \gtrsim 3$. Also, each code would need a different set of zero-point offsets, which would add a level of inconsistency in the input photometry. We therefore opted not to modify the zeropoints or modify the templates based on the spectroscopic redshifts.

3.1. Spectroscopic Redshifts

In order to test the accuracy of our photometric redshifts as well as to combine the results from the individual codes together, we require a highly vetted spectroscopic redshift catalog. We use a compilation of publicly available spectroscopic redshifts obtained from various facilities/sources in the UVCANDELS fields. The final spectroscopic reference sample used in this analysis is assembled from a combination of the 3D-HST (Brammer et al. 2012; Momcheva et al. 2016), zCOSMOS (Lilly et al. 2007, 2009), hCOSMOS (Damjanov et al. 2018), PRIMUS (Coil et al. 2011), MOSDEF (Kriek et al. 2015), DEIMOS 10K (Hasinger et al. 2018), DEEP2 (Newman et al. 2013), DEEP3 (Cooper et al. 2011, 2012), MUSE-Wide (Herenz et al. 2017), MUSE-HUDF (Inami et al. 2017), K20 (Mignoli et al. 2005), C3R2 (Masters et al. 2019; Stanford et al. 2021), LEGA-C (van der Wel et al. 2016), VVDS (Le Fèvre et al. 2013), VUDS (Le Fèvre et al. 2015), VANDELS (McLure et al. 2018; Pentericci et al. 2018), GMASS (Kurk et al. 2013), FMOS-COSMOS (Silverman et al. 2015), FIREWORKS (Wuyts et al. 2008), GOODS-MUSIC (Grazian et al. 2006), PEARS (Straughn et al. 2009; Ferreras et al. 2009), GRAPES-HUDF (Hathi et al. 2009; Pasquali et al. 2006), LCIRS (Doherty et al. 2005) spectroscopic surveys as well as compilations from the following publications: Balestra et al. (2010); Barger et al. (2008); Cristiani et al. (2000); Croom et al. (2001); Daddi et al. (2004); Huang et al. (2009); Krogager et al. (2014); Ravikumar et al. (2007); Roche et al. (2006); Strolger et al. (2004); Treister et al. (2009); Trump et al. (2009, 2011, 2013, 2015); Vanzella et al. (2008, 2009); van der Wel et al. (2005); Wirth et al. (2015); Wolf et al. (2004); Wuyts et al. (2009); Yoshikawa et al. (2010), including some spectroscopic redshifts provided to our team via private communication.

For our spectroscopic reference sample, we only include those redshifts with the highest data quality flags from the individual papers, and those 3D-HST grism redshifts with good grism data quality flags (`use_zgrism=1`). We omit sources with X-ray detections to avoid AGN contaminants, (Xue et al. 2016, D. Kocevski 2023, private communication), which amounts to a total of 858 objects excluded. To avoid potential confusion from neighbors in ground-based spectroscopy, we also exclude any sources that have a relatively bright neighbor, defined as a source within $3''$ and within 2 mag or brighter in F160W. As a final measure to ensure only the highest quality redshifts remain, we visually inspect all sources with photometric redshift outliers (defined as $|z_{\text{spec}} - z_{\text{phot}}|/(1 + z_{\text{spec}}) > 0.15$) and remove those with anomalous behavior affecting the input photome-

try. These are typically sources contaminated by very bright, extended sources not caught by the automated neighbor cut, but also include sources with other contaminants, including stars or diffraction spikes. The final visual vetting removes 0.5% of all available redshifts. After the vetting procedure, we compile a spectroscopic redshift catalog including 8,081 redshifts in total over the four CANDELS fields.

The spectroscopic redshifts from this compilation (limited to those available publicly) are included in the photometric redshift catalog released as part of this work (see Section 5 and Table 2).

3.2. Combining Photometric Redshifts

In order to combine the results from the 5 individual runs into a single estimate for the photometric redshift, we add together the individual probability distribution functions, $P(z)$, following the procedure outlined in Dahlen et al. (2013) (see their Section 5.2).

Before combining the individual $P(z)$, it is imperative to ensure that the photometric redshift accuracy estimated from the individual codes is consistent and representative of the actual sample of galaxies for which the photometric redshifts are derived. One common check is to compare the 1σ uncertainty from the $P(z)$ with that derived directly from the offsets with respect to the spectroscopic reference sample (e.g., Ilbert et al. 2009). In the cases where the $P(z)$ underestimates (overestimates) the statistical errors from the spectroscopic sample com-

parison, a smoothing (sharpening) can be applied to the $P(z)$ to ensure that the error estimates on the photometric redshifts are accurate and consistent (e.g., Dahlen et al. 2013).

Similar to Dahlen et al. (2013), we find that the individual codes used in our analysis underestimate their confidence intervals, i.e. fewer than 68.3% (1σ) of galaxies with known spectroscopic redshifts fall within their 68.3% confidence intervals from the photometric redshift probability distributions $P(z)$. Hence, to alleviate this, we iteratively smooth each $P(z)_i$ for code i and redshift bin j by

$$P(z_j)_i = 0.25P(z_j-1)_i + 0.5P(z_j)_i + 0.25P(z_j+1)_i \quad (1)$$

until 68.3% of the known spectroscopic redshifts fall within the smoothed $P(z)$ 68.3% confidence intervals. We perform this smoothing procedure for each code separately, as each code requires a different number of smoothing iterations. Next, we add the smoothed probability distributions from each code together and renormalize. Similar to Dahlen et al. (2013), we find that these resulting probability distributions after combining tend to overestimate the confidence intervals, and hence we apply a sharpening according to $P(z_j)_i^{1/\alpha}$, where the exponent α is chosen to ensure 68.3% of the spectroscopic redshifts fall within the 68.3% confidence intervals. This results in a single $P(z)$ that combines the knowledge for all individual fitting codes with a corresponding error (or confidence interval) that is statistically consistent with the spectroscopic reference sample used for calibration. The final probability distributions are on a redshift grid of $z = 0 - 12$ in steps of 0.01. Figure 1 shows an example of this combination procedure for an individual source.

We note that when the photometric redshift codes fail, they output a redshift of ~ 0 at high probability, which can affect the combined redshifts. For example, a failure mode of EAZY returns a redshift of ~ 0.01 with 100% confidence in the $P(z)$. This throws off the combined $P(z)$ distribution, resulting in a redshift at $z < 0.06$ due to the high confidence over a small redshift range. Since the number of expected galaxies at $z < 0.06$ in the field of view is extremely small, we truncated the redshift catalog at $z = 0.06$ to avoid cases with code failures.

We identify multiple peaks in each $P(z)$ as those with peak and prominence at least 10% that of the main peaks, and with no higher peak within $0.06(1+z)$. The confidence intervals for each peak are calculated from the minimums between two neighboring peaks. We record up to 3 separate redshift peaks in the final photometric redshift catalogs, sorted by height (z_{peak} , $z_{\text{peak}2}$, $z_{\text{peak}3}$). Overall, we find that 20.5% of sources

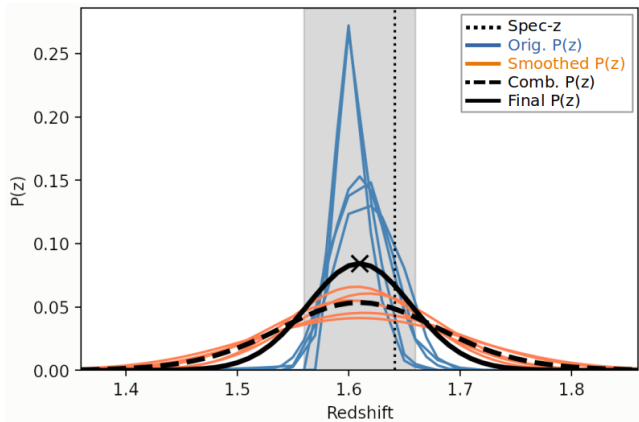


Figure 1. An example of the photometric redshift probability distribution combination process for an example source (COSMOS-697: $z_{\text{spec}} = 1.6418$; $z_{\text{phot}} = 1.61 \pm 0.05$). Blue curves show the $P(z)$'s from the individual codes, orange curves show these $P(z)$'s after smoothing, and the black curves show the final combined $P(z)$ before (dashed) and after (solid) the final sharpening procedure. The final photometric redshift (cross symbol) and confidence intervals (shaded gray region) of the final $P(z)$ are shown, along with the spectroscopic redshift (dotted line).

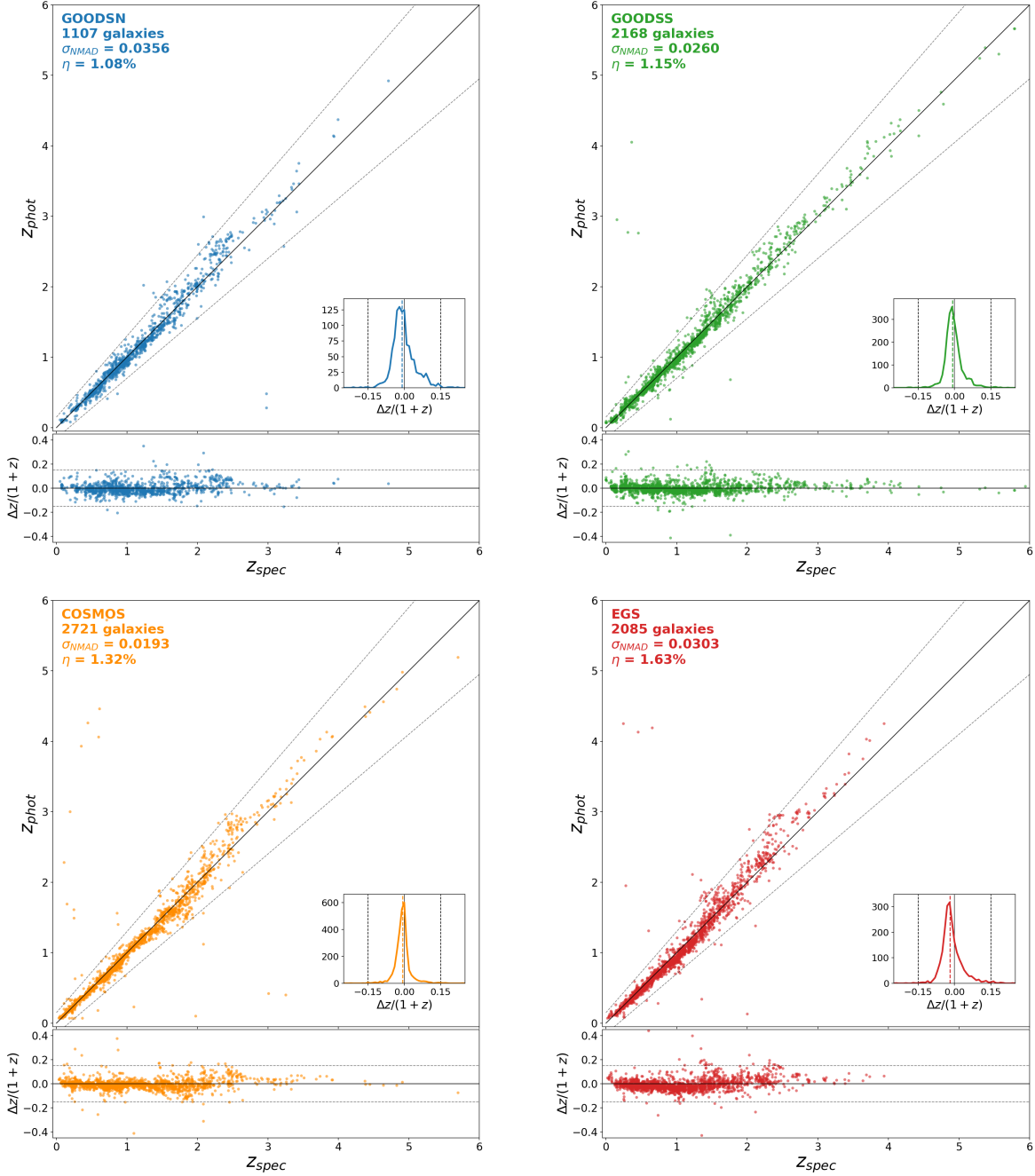


Figure 2. Comparison of the performance of the photometric redshifts with the spectroscopic sample for each of the individual fields. The key statistics, i.e., the scatter (σ_{NMAD}) and the outlier fraction ($\eta = |\Delta z|/(1+z) > 0.15$) are reported in the *upper left* corner. The inset shows the distribution of the fractional differences between the photometric and spectroscopic redshifts. The *dotted* lines show the outlier criterion: $z_{\text{phot}} = z_{\text{spec}} \pm 0.15(1 + z_{\text{spec}})$ and the *dashed* lines show the median of the distribution.

have 2 peaks, and 3.4% have 3 peaks. Typically, the final photometric redshift and its associated error is recorded as the median and 68.3% confidence intervals of the $P(z)$. However, for the $\sim 1\%$ of sources that have multiple peaks with the main peak at $z < 0.1$, we instead record the second peak as the final photometric redshift,

as the main peak could be due to some codes failing to find a good fit.

The final photometric redshifts along with their errors are provided in the photometric redshift catalog (see Table 2) and the full redshift probability distributions are also provided separately (see Table 3).

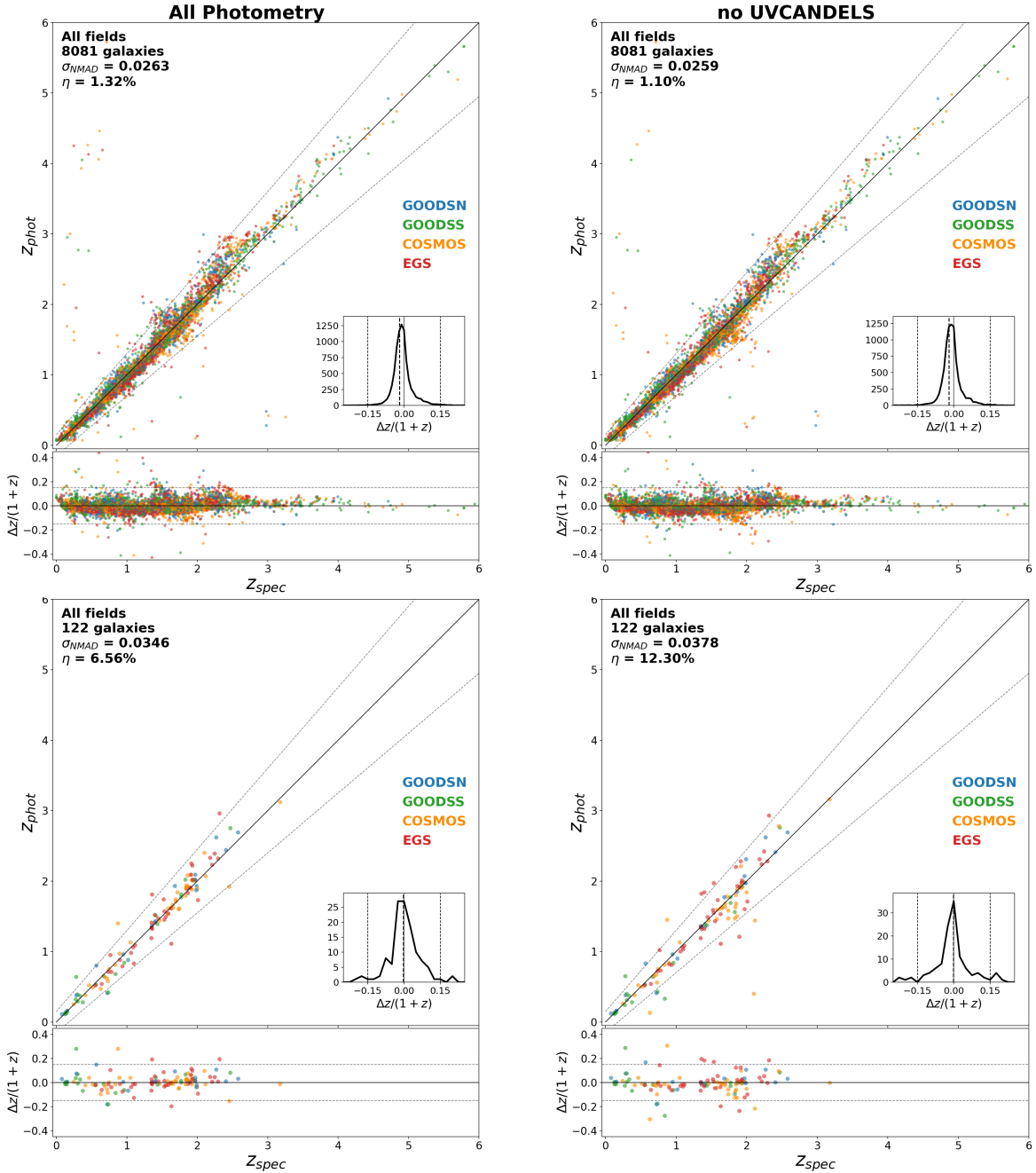


Figure 3. An aggregate comparison between the photometric and spectroscopic redshifts for all four CANDELS fields combined. The *left column* plots show the comparison where all available filters were included in the photometric redshift fitting, where as the *right column* plots show the same without using filters from the UVCANDELS program (i.e. F275W/F435W for COSMOS and EGS; F275W for GOODSN and GOODSS). The *top row* plots include all sources, where as the *bottom row* plots only shows sources with multiple peaks in their probability distributions $P(z)$ and with $\text{SNR} > 3$ in F275W. The improvement of the photometric redshift by including the UV photometry is evident in this case, reducing both σ_{NMAD} and η for sources detected in the UV or that previously had multiple peaks in $P(z)$.

3.3. Quality of Resultant Redshifts

Figure 2 shows the comparison between the photometric redshifts and spectroscopic redshifts for each CANDELS field, as well as the overall scatter (NMAD; nor-

malized median absolute deviation) defined by

$$\sigma_{\text{NMAD}} = 1.48 \times \text{median}(|\Delta z| / (1 + z_{\text{spec}})) \quad (2)$$

and outlier fraction η , where

$$\eta = |\Delta z| / (1 + z_{\text{spec}}) > 0.15. \quad (3)$$

Figure 2 shows the performance in each individual field. We find that η is lower for fields with more filters (e.g. COSMOS has the lowest η). On the other hand, we see the best σ_{NMAD} for GOODS-N and GOODS-S, which have the most filters and deepest imaging. Overall, EGS performs the worst with the fewest filters, but still have relatively low η and σ_{NMAD} given the excellent coverage.

The top left panel of Figure 3 shows the performance on the combined sample across all fields. We obtain an average σ_{NMAD} of 0.0263 and outlier fraction η of 1.32%. This is within family of the other photometric redshifts determined for the CANDELS fields (e.g. Dahlen et al. 2013; Skelton et al. 2014; Bezanson et al. 2016; Kodra et al. 2023). We note that the quality of σ_{NMAD} and η depends on the quality of the spectroscopic sample being compared to. Therefore, it is not useful to carefully compare the values of σ_{NMAD} and η between studies of the same fields determined from different spectroscopic samples. In fact, we could probably improve our η further by careful inspection of all the spectroscopic data, but that is out of the scope of this paper. On the other hand, we can investigate the improvements in photometric redshifts with the addition of the UVCANDELS data with the same spectroscopic sample.

3.4. Improvement of Photometric Redshifts with UVCANDELS data

Aside from the fiducial case (all photometry), in order to quantify the impact of including the new UV photometry from UVCANDELS, we repeat the analysis of estimating photometric redshifts for an additional scenario without including the UVCANDELS photometry, i.e., no F275W for all fields and no F435W for COSMOS and EGS. The results from this test are shown in Figure 3.

As evident from Figure 3, high-fidelity photometric redshift estimates can be obtained with and without the inclusion of UVCANDELS photometry (i.e. F275W/F435W); the scatter and outlier fraction are within 0.004 and 0.22%, respectively. This is because the vast majority of galaxies in the catalogs do not have detections in the UV, either because they are too faint, or because they are at high redshift. Unlike in the UVUDF where the UV limits significantly improved the photometric redshifts (Rafelski et al. 2015), the depth of the UVCANDELS data only provide modest limits for non-detections, which do not significantly help the redshift determinations which already are based on many filters. Additionally, these fields have ground-based u -band data as well, already providing useful limits on non-detections at similar wavelengths, and further re-

ducing the benefits of the F275W and F435W from UVCANDELS for photometric redshifts.

For a more useful measure of the improvement provided by the UV data to the photometric redshifts, we limit ourselves to sources with significant F275W fluxes. The *bottom row* in Figure 3 shows only those sources with multiple $P(z)$ peaks and $\text{SNR} > 3$ in F275W. In this case, the improvement in the photometric redshift quality when including UV data is significantly more evident; the scatter and outlier fraction falls by 0.003 and 5.7%, respectively. The percentage of sources with multiple peaks also decreases from 23.4% to 20.5% after including the UV data.

4. GALAXY PHYSICAL PROPERTIES

The star-formation history (SFH) represents one of the core components for defining a stellar population for a galaxy and consequently, its SED. Traditionally, galaxy SED modeling tools have typically implemented fixed, functional forms to parameterize galaxy SFHs, such as exponentially rising/declining, delayed exponential, constant, short bursts, or some linear combination of thereof. However, modern SED modeling tools have evolved beyond the basic functional forms to now allow for more flexible, and even non-parametric forms for the galaxy SFH. Several recent studies have investigated the differences in the stellar physical parameters estimated from parametric and non-parametric approaches (e.g., Lower et al. 2020; Pacifici et al. 2023; Kaushal et al. 2024; Jain et al. 2024) and the general consensus from comparisons prefers the non-parametric or flexible SFH approach, which returns more accurate physical parameters (e.g., Iyer & Gawiser 2017; Iyer et al. 2019; Leja et al. 2019).

With the rich UVCANDELS+CANDELS multi-wavelength photometric dataset and redshifts described in Section 2.2 and 3 respectively, here we investigate the impact of the SFH parameterization on the inferred galaxy physical properties from the observational perspective. In this work, we implement two parallel approaches for modeling galaxy SEDs and estimating galaxy physical parameters: (i) a modern approach that facilitates flexible SFHs, and (ii) a fiducial approach that utilizes traditional, fixed functional SFHs. In the following sections, we describe our methodology for each of these approaches. For both, we use the photometric dataset described in Section 2.2 for the SED modeling.

4.1. Fitting flexible SFHs with DENSE BASIS

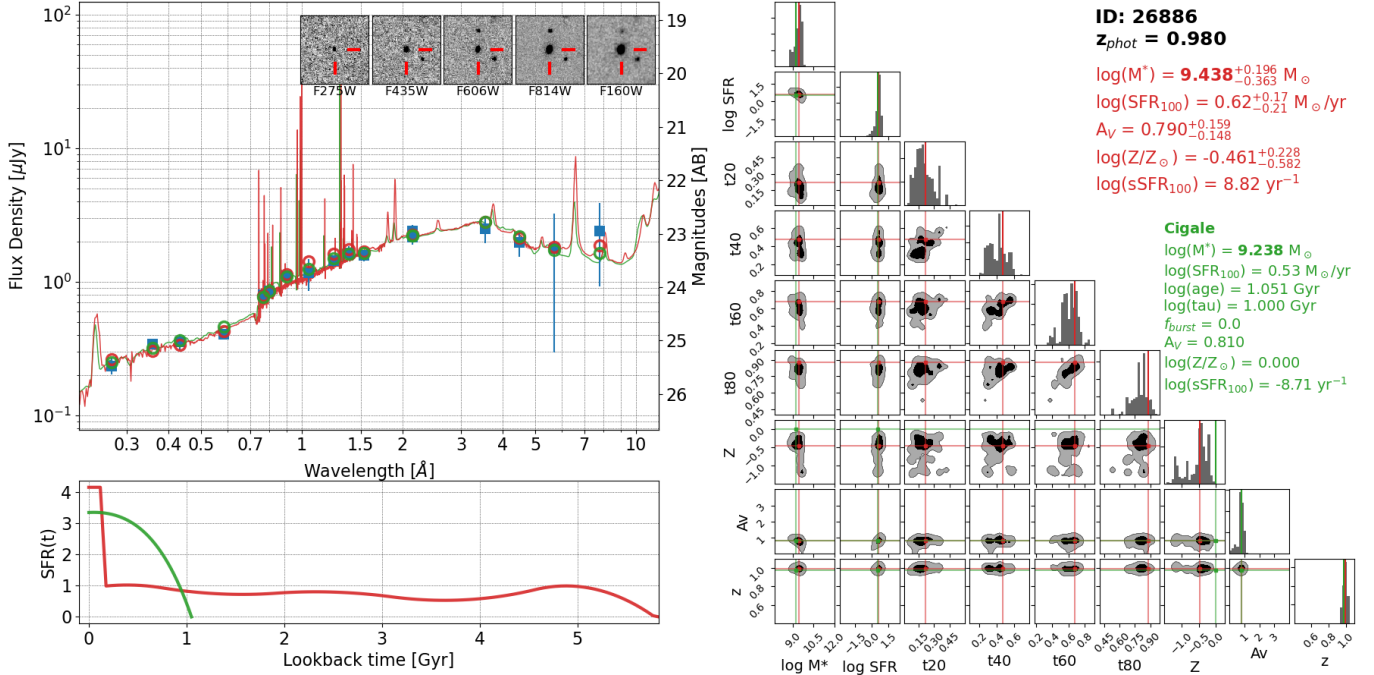


Figure 4. The SED modeling shown for an example galaxy (GOODSN-26886). The *top left* panel shows the observed photometry (shown in *blue*) along with the best-fit model template from the flexible (DENSE BASIS, in *red*) and fixed (CIGALE, in *green*) SFH assumptions. The insets show $5'' \times 5''$ postage stamps of the galaxy in the respective filters. The *bottom left* panel shows the best-fit SFH for both cases demonstrating how the flexible-form SFH captures SF at earlier times that is missed by the fixed-form approach, while both return excellent overall fit to the observed photometry. For the DENSE BASIS result, a corner plot with the posterior distributions of the free parameters is shown on the *right* along with the best-fit parameter values for both cases.

For the flexible SFH approach, we use the SED modeling tool DENSE BASIS⁵ (Iyer et al. 2019), which uses Gaussian Process Regression to model highly flexible SFHs. The key advantage of the Gaussian Process (GP) based formalism is its ability to encode maximum amount of information in the complex galaxy SFHs using a minimal number of parameters. As demonstrated in Iyer et al. (2019), this formalism minimizes the bias in estimating galaxy SFHs at all lookback times, compared to the parametric (functional) approaches.

4.1.1. Defining the SFHs

The galaxy SFHs in DENSE BASIS are described using a fixed number of “shape” parameters (N). These shape parameters (t_X) are N lookback times at which the galaxy formed equally spaced quantiles of its total mass (see Iyer et al. 2019 for a more detailed description). For this work, we adopt $N = 4$ shape parameters for describing the galaxy SFHs with 4 t_X parameters: t_{20} , t_{40} , t_{60} , t_{80} representing the lookback times⁶

⁵ <https://dense-basis.readthedocs.io/en/latest/>
<https://dfm.io/python-fsps/>

⁶ These lookback times are defined as the fraction of the age of the universe (at the given redshift for a galaxy).

at which the galaxy assembled 20%, 40%, 60%, 80% of its total stellar mass, respectively. We choose $N = 4$ for the GP-based SFH parameterization as it allows for sufficient flexibility (Iyer et al. 2019) while minimizing the computation time for the SED modeling.

Furthermore, we allow the GP-based SFHs to have a “de-coupled” star-formation episode over the most recent 100 Myr, which still retains continuity with the rest of the SFH but allows for further flexibility in fitting any recent star-formation traced by the newly added rest-frame UV data from UVCANDELS.

4.1.2. Galaxy model template library

The galaxy model templates in DENSE BASIS are defined using the FSPS⁷ (Flexible Stellar Population Synthesis; Conroy et al. 2009; Conroy & Gunn 2010a) library, which includes a self-consistent prescription for both the stellar continuum as well as nebular emission. The nebular emission lines and continuum implementation in FSPS is based on the CLOUDY models from Byler et al. (2017). We also use the built-in Draine & Li (2007) model for dust emission.

⁷ <https://github.com/cconroy20/fsps>

For this analysis, we assume a Chabrier (2003) IMF, which is a well-established choice when fitting the SEDs of a general galaxy population, particularly at higher redshifts where galaxies tend to be relatively more star-forming and have lower metallicities (see e.g., Chabrier et al. 2014; Hopkins 2018). We adopt the Madau (1995) model for IGM absorption, and the Calzetti et al. (2000) dust attenuation law, which couples the attenuation for young and older stars (i.e., assumes the same dust attenuation for the nebular and stellar components) with one free parameter: A_V , the V -band dust attenuation. We also assume the gas-phase metallicity to be equal to the stellar metallicity (left as a free parameter), and the ionization parameter for the nebular gas is left as default ($\log U = -2$).

The template redshifts are set to the galaxy’s photometric redshifts defined in Section 3. During fitting, a nominal error of $\delta(z) = 0.025 \cdot z/(1+z)$ is assumed to ensure a robust estimation for the galaxy physical parameters.

4.1.3. Priors and Parameter estimation

Ultimately, we perform the fitting with 8 free parameters: the galaxy stellar mass (M^*), star-formation rate (SFR; over the recent 100 Myr), the stellar dust attenuation (A_V), the stellar metallicity (Z^*), and the 4 t_X parameters ($t_{20}, t_{40}, t_{60}, t_{80}$) that define the galaxy SFH.

We jointly define the prior for M^* and SFR as the specific star-formation rate (sSFR=SFR/ M^*), which is assumed as a uniform (flat) prior spanning a range of $\log(\text{sSFR}) = -12$ to -7 yr^{-1} . We adopt uniform (flat) prior for A_V spanning from $A_V = 0$ to 4, and for Z^* over $\log(Z/Z_\odot) = -1.5$ to 0.25. For the GP-based SFH parameters, i.e., the t_X lookback times, we adopt a Dirichlet prior with $\alpha = 5$ as per the recommendation from Iyer et al. (2019), which leads to a distribution of parameters that is well-matched to galaxies in simulations.

We perform parameter estimation for DENSE BASIS in two ways: (i) For each galaxy, a likelihood is computed from the sufficiently large number of model SEDs realized in the pre-generated grid library with parameters drawn according to the priors described above. This results in a posterior distribution for each of the free parameters. The posterior medians and 1σ (68%) percentiles are then used to define the best-fit parameters and the associated errors. (ii) A simpler, frequentist approach is also implemented that uses the (single) SED from the pre-generated library with the minimum χ^2 value to define the best-fit parameters, with no uncertainties reported.

The estimates from the full posterior analysis are generally more robust and preferred over the simple mini-

mum χ^2 result, but we provide both for completeness and as a consistency check (see Table 4). Figure 4 demonstrates the modeling for an example galaxy along with the full posterior distributions for the free parameters. The full mass-redshift distribution for each of the fields is shown in Figure 5.

4.2. Fitting fixed SFHs with CIGALE

For our fiducial approach, we use the traditional approach of using fixed, functional forms for the galaxy SFHs. In this case, we implement the CIGALE⁸ (Code Investigating GALaxy Emission; Boquien et al. 2019; Burgarella et al. 2005; Noll et al. 2009) tool for the estimation of the galaxy physical properties.

4.2.1. Defining the SFHs

For the galaxy SFH parameterization within CIGALE, we adopt a delayed-exponential functional form⁹ with an additional possibility for an episode of recent star-burst (similar as with DENSE BASIS) with an exponentially declining functional form. The SFH is parameterized with an overall age (t_{age}) and an e -folding timescale (τ) for the main stellar population, along with an age (t_{burst}) and an e -folding timescale (τ_{burst}) for the burst episode as well as the fraction of mass formed in the burst phase (f_{burst}).

In order to keep the computational times manageable, we fix the burst population’s t_{burst} and τ_{burst} parameters to 10 Myr and 50 Myr, respectively, while the remaining parameters (t_{age} , τ_{age} , and f_{burst}) are varied freely.

4.2.2. Galaxy model template library

Here, we use the Bruzual & Charlot (2003) stellar population models, along with the prescription for nebular emission (both emission line and continuum) included within CIGALE, which is based on Inoue (2011). We note that the IGM prescriptions between CIGALE and DENSE BASIS (Section 4.1) are not identically similar, which is a technical limitation as these are the only prescriptions available within the respective codes. We use the dust emission model from Dale et al. (2014) included in CIGALE.

For this analysis, we assume a Chabrier (2003) IMF and the prescription from Meiksin (2006) is used for the IGM absorption. Same as the flexible SFH case, we adopt the Calzetti et al. (2000) dust law (which assumes same attenuation for young and older stars (and hence the nebular and stellar dust components) parameterized by the free parameter A_V or $E(B-V) = A_V/4.05$.

⁸ <https://cigale.lam.fr/>

⁹ $\text{SFR}(t) \propto t e^{-t/\tau}$

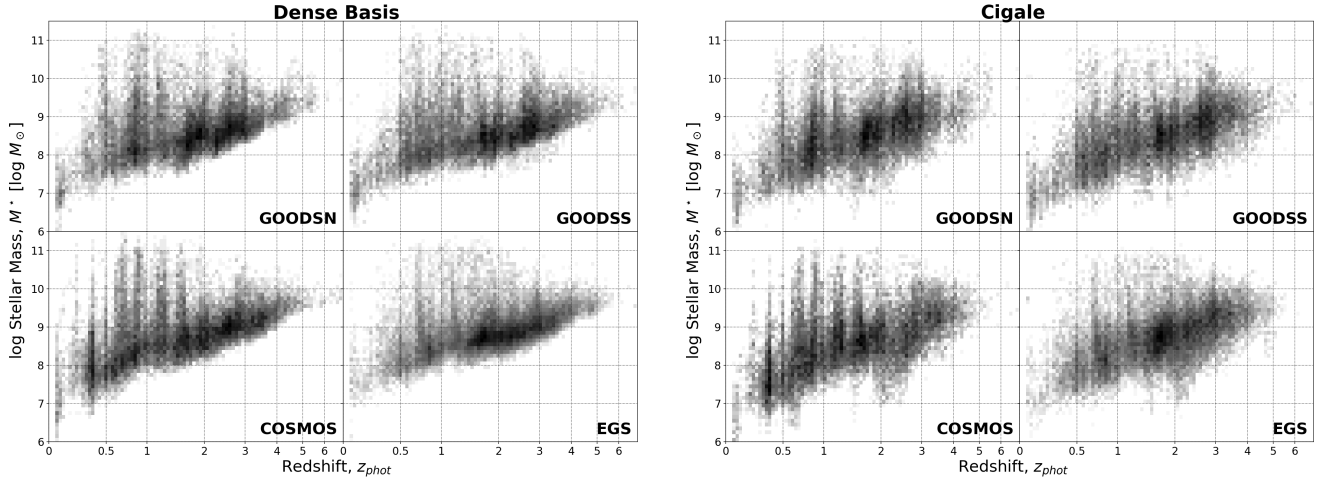


Figure 5. The mass distribution as a function of redshift for each field, with the masses estimated using the flexible (DENSE BASIS, *left panel*) and fixed (CIGALE, *right panel*) SFH assumptions.

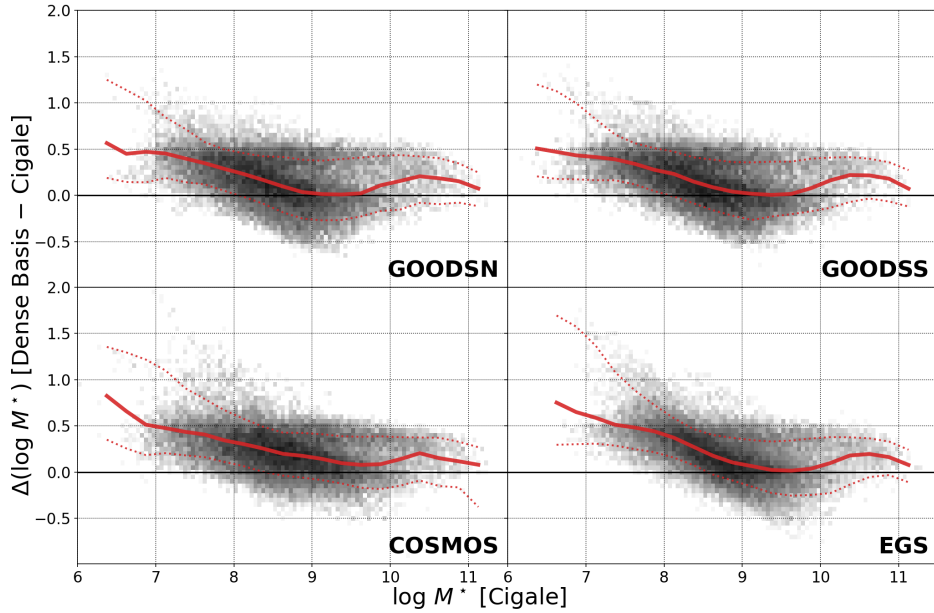


Figure 6. The difference between the galaxy stellar masses estimated from flexible (DENSE BASIS) and fixed (CIGALE) SFH approaches. The *red* curves show the running median (*solid*) and the 68% (1σ) percentile for the population. Even when fitting the same photometric dataset with consistent assumptions, the inferred stellar masses are significantly impacted by the parameterization of the galaxy SFH during SED modelling.

Here, the gas-phase metallicity is assumed to be solar and the gas ionization parameter is left at its default value ($\log U = -2$).

The template redshifts are set to the galaxy’s photometric redshifts defined in Section 3. In the case of CIGALE, since all models are generated at the input redshifts, the galaxy redshifts are treated as exact, albeit rounded to 2 decimals to manage computation time.

4.2.3. Parameter estimation

For this CIGALE implementation, we have 7 free parameters: the galaxy stellar mass (M^*), star-formation

rate (SFR), stellar dust attenuation (A_V), stellar metallicity (Z^*) and the SFH-related parameters, t_{age} , τ_{age} , and f_{burst} .

For the main stellar population in the SFH, the age, t_{age} , is allowed to vary over a grid of 21 points from 10 Myr to the age of the universe and similarly, τ_{age} is varied freely over a grid spanning over 30 Myr to 30 Gyr. For the burst component, f_{burst} is allowed to vary (over gridded values from 0 to 1). Lastly, the dust attenuation parameter $E(B - V) = A_V/4.05$ is varied over $[0, 1.2]$ and the stellar metallicity over $\log(Z/Z_\odot) = [-2.3, 0.4]$.

The best-fit parameters are estimated by performing a minimum χ^2 search over a template library generated from the full grid of free parameters. As part of the output, an instantaneous as well as a 100 Myr averaged SFR is reported (see Table 5). The resulting best-fit solutions from both the flexible (DENSE BASIS) and fixed (CIGALE) approaches for an example galaxy is shown in Figure 4 while the full mass-redshift distribution for each field is shown in Figure 5.

4.3. The impact of the SFH assumption on parameter estimates

From a statistical perspective, the SED modeling with either of the approaches (flexible/DENSE BASIS or fixed/CIGALE) are relatively robust with no significant systematic biases in the fitting residuals. As illustrated in Figure 4 with an example galaxy, the best-fit model template from both methodologies represents a qualitatively good fit to the observed photometry.

However, a population comparison of the best-fit parameters reveals significant systematic biases in even the most basic physical property, the galaxy stellar mass. Figure 6 shows the difference in the stellar mass inferred from the two approaches and it is evident that the masses estimated from the flexible SFH assumption (DENSE BASIS) are systematically higher, particularly at the low-mass end. For typical galaxies ($\sim 10^9\text{--}10^{10} M_\odot$), the stellar masses are in good agreement regardless of the SFH parameterization. However, below $\sim 10^9 M_\odot$, the flexible-SFH stellar masses get increasingly biased by as much as 0.5 dex at $\sim 10^7 M_\odot$. Similarly, at the high-mass end ($\gtrsim 10^{10} M_\odot$), the masses from DENSE BASIS are also systematically higher, albeit only by ~ 0.2 dex.

This discrepancy in the estimated stellar masses due to different SFH assumptions is not new and has already been reported in the literature (e.g., Leja et al. 2019; Lower et al. 2020; Jain et al. 2024). Our results here are broadly consistent with the previous findings. From comparisons to simulated galaxies, it is clear that the stellar masses estimated using flexible SFHs are closer to the true value and it is the fixed-form SFHs that underestimate the stellar masses (e.g., Lower et al. 2020). This is due to their inability to simultaneously capture the multiple episodes of star-formation and other gradual changes in the SFHs. This effect is also evident in the example shown in Figure 4, where the fixed SFH (from CIGALE; in *green*) is missing the early episode of star-formation captured by the flexible SFH (from DENSE BASIS; in *black*). This effect is amplified particularly at the lower mass end ($\lesssim 10^9 M_\odot$) where galaxies tend to have more chaotic, bursty SFHs with multiple

episodes of prominent star-formation activity, which can contribute relatively large differences in their galaxies' stellar masses (e.g., Emami et al. 2019). On a similar note, at higher masses, it is likely that the functional form of the fixed SFHs is missing the extended periods of star-formation activity due to the choice of parameterization, again resulting in underestimated masses.

5. CATALOG DESCRIPTIONS

From the analysis presented here, we produce catalogs listing new photometric redshifts as well as galaxy physical properties for the four CANDELS fields covered by UVCANDELS (GOODS-N, GOODS-S, COSMOS, EGS). These catalogs will be publicly released via MAST ([doi:10.17909/8s31-f778](https://doi.org/10.17909/8s31-f778)¹⁰). The full output is delivered with the following catalogs:

- (i) A catalog presenting the photometric redshifts from Section 3 (see column description in Table 2);
- (ii) The full probability distribution, $P(z)$, for the photometric redshifts from Section 3 (see column description in Table 3);
- (iii) Catalogs for each field listing the best-fit galaxy physical properties estimated using DENSE BASIS with the flexible SFH assumption from Section 4.1 (see column description in Table 4); and
- (iv) Per-field galaxy physical properties catalogs from CIGALE (fixed SFH assumption) from Section 4.2 (see column description in Table 5).

6. SUMMARY

We present a set of new measurements for photometric redshifts and galaxy physical parameters for over 150,000 galaxies in four of the five CANDELS fields (GOODS-N, GOODS-S, COSMOS, EGS; combined area of ~ 430 arcmin²) covered by the recent *Hubble* Treasury program, UVCANDELS. In this work, we utilize the UV-to-IR photometric dataset available for these fields from a combination of the existing *HST* optical/NIR, *Spitzer* mid-IR, and other ancillary ground-based imaging as well as the newly acquired WFC3/UVIS F275W

¹⁰ <https://archive.stsci.edu/hlsp/uvcandels>

Table 2. Column descriptions for the photometric redshift catalog

#	Parameter	Description
1	<code>field</code>	The CANDELS field
2	<code>ID</code>	The CANDELS ID
3	<code>RA</code>	Right ascension
4	<code>DEC</code>	Declination
5	<code>photz</code>	Best photometric redshift
6	<code>l68</code>	Lower 68.3% confidence interval of <code>photz</code>
7	<code>u68</code>	Upper 68.3% confidence interval of <code>photz</code>
8	<code>zpeak</code>	Highest $P(z)$ peak
9	<code>zpeak_l68</code>	Lower 68.3% confidence interval of <code>zpeak</code>
10	<code>zpeak_u68</code>	Upper 68.3% confidence interval of <code>zpeak</code>
11	<code>zpeak2</code>	Second highest $P(z)$ peak
12	<code>zpeak2_l68</code>	Lower 68.3% confidence interval of <code>zpeak2</code>
13	<code>zpeak2_u68</code>	Upper 68.3% confidence interval of <code>zpeak2</code>
14	<code>zpeak3</code>	Third highest $P(z)$ peak
15	<code>zpeak3_l68</code>	Lower 68.3% confidence interval of <code>zpeak3</code>
16	<code>zpeak3_u68</code>	Upper 68.3% confidence interval of <code>zpeak3</code>
17	<code>photz_med</code>	Median of the $P(z)$
18	<code>photz_med_l68</code>	Lower 68.3% confidence interval of <code>photz_med</code>
19	<code>photz_med_u68</code>	Upper 68.3% confidence interval of <code>photz_med</code>
20	<code>specz</code>	The spectroscopic redshift
21	<code>specz_ref</code>	The source of the spectroscopic redshift

NOTE—The `photz` column is the best redshift to use, and generally consists of the median of the $P(z)$ (i.e. `photz_med`). However, sometimes if the first peak is at low redshift ($z < 0.1$), it is instead the second $P(z)$ peak (i.e. `zpeak2`) to avoid issues with the photometric redshift software as described in the text. Missing or irrelevant values are set to -99.

and ACS/WFC F435W (for COSMOS and EGS) imaging from UVCANDELS, to model the galaxy SEDs using state-of-the-art fitting tools.

Our key findings are as follows:

- The inclusion of UV photometry significantly improves the photometric redshift for sources with significant UV detections and degenerate redshift solutions. After adding UV photometry when measuring the redshifts, we find significantly lower outlier fractions for sources with $\text{SNR} > 3$ in

Table 3. Column descriptions for the catalog presenting the photometric redshift probability distribution $P(z)$

#	Parameter	Description
1	<code>field</code>	The CANDELS field
2	<code>ID</code>	The CANDELS ID
3	<code>RA</code>	Right ascension
4	<code>DEC</code>	Declination
5	<code>pz</code>	$P(z)$

NOTE—The third column consists of the photometric redshift probability distribution $P(z)$ on a redshift grid from $z = 0 - 12$ in steps of 0.01. This probability function is useful when considering how robust a photometric redshift is.

F275W and multiple peaks in their probability distributions, $P(z)$.

- When modeling galaxy SEDs, the typical assumption of a fixed, functional form for the galaxy SFH systematically biases the measurement of even the most basic physical parameter – the galaxy stellar mass – at both the low- ($\lesssim 10^9 M_\odot$) as well as the high-mass ($\gtrsim 10^{10} M_\odot$) end. We find the fixed-form SFHs to underestimate the stellar mass by as much as ~ 0.5 dex at $10^7 M_\odot$ and ~ 0.2 at $10^{10.5} M_\odot$.
- This underestimation for the stellar mass is mainly driven by the inability of the fixed-form SFHs to simultaneously capture the major star-formation episodes as well as the prolonged lower-level star-formation and/or other gradual changes in the galaxy SFHs.

The final catalogs presenting the photometric redshifts and physical parameters will be publicly available via the MAST archive¹¹.

¹¹ <https://archive.stsci.edu/hlsp/uvcanfels>

Table 4. Column descriptions for the catalog presenting the galaxy physical properties computed from DENSE BASIS

#	Parameter	Description
1	ID ^a	Identification number
2	RA ^a	Right ascension
3	DEC ^a	Declination
4	photz	Photometric redshift used (from Table 2)
5	delz	Error on photometric redshift (assumed)
6	nbands	Number of photometric bands used for fitting
Parameter estimates from the posterior distribution		
7–9	logM ^b	Galaxy stellar mass estimate [$\log M_{\odot}$]
10–12	logSFR ^b	Star-formation rate [$\log M_{\odot}/yr$]
13–15	Av ^b	Dust attenuation (V-band) [mag]
16–18	logZsol ^b	Stellar metallicity [$\log Z_{\odot}$]
18–21	t20 ^b	Time ^c when 20% of galaxy mass was formed
22–24	t40 ^b	Time ^c when 40% of galaxy mass was formed
25–27	t60 ^b	Time ^c when 60% of galaxy mass was formed
28–30	t80 ^b	Time ^c when 80% of galaxy mass was formed
31–33	color_nuvu ^b	Rest-frame NUV-U color
34–36	color_nuvr ^b	Rest-frame NUV-R color
37–39	color_uv ^b	Rest-frame U-V color
40–42	color_vj ^b	Rest-frame V-J color
43–45	color_rj ^b	Rest-frame R-J color
46	flags	Quality flags ^d
Parameter estimates from the minimum- χ^2 model		
47	logM_chi2	Galaxy stellar mass estimate [$\log M_{\odot}$]
48	logSFR_chi2	Star-formation rate [$\log M_{\odot}/yr$]
49	Av_chi2	Dust attenuation (V-band) [mag]
50	logZsol_chi2	Stellar metallicity [$\log Z_{\odot}$]
51	t20_chi2	Time ^c when 20% of galaxy mass was formed
52	t40_chi2	Time ^c when 40% of galaxy mass was formed
53	t60_chi2	Time ^c when 60% of galaxy mass was formed
54	t80_chi2	Time ^c when 80% of galaxy mass was formed
55	color_nuvu_chi2	Rest-frame NUV-U color
56	color_nuvr_chi2	Rest-frame NUV-R color
57	color_uv_chi2	Rest-frame U-V color
58	color_vj_chi2	Rest-frame V-J color
59	color_rj_chi2	Rest-frame R-J color
60	chi2	χ^2 value for the minimum- χ^2 solution
Model magnitudes from the best-fit template ^e		
61–69	model_Lnu_rest*	Model template fluxes for rest-frame Johnson filters (FUV, NUV, <i>UBVR IJK</i>) [μJy]
70–	model_Fnu_* ^f	Model template fluxes for observed photometric bands [μJy]

^aThe galaxy ID number, RA and DEC are consistent with that from the CANDELS photometric catalogs and the catalogs for each field are provided separately.

^bFor these columns, each has two additional columns named *.16 and *.84 denoting the 1σ (68%) confidence interval for the best estimate.

^cThe time is given as the fraction of the age of the universe (at the redshift of the galaxy).

^dQuality flags: 1=invalid fit (**nan** for mass estimate); 2=large SFR uncertainties ($\Delta(\log SFR) > 2$); 3= objects flagged as stars in photometry catalog (**CLASS_STAR**>0.5); 4=poor fit/large χ^2 (>1000).

^eThese model magnitudes are computed for the best-fit parameters estimated from the full Bayesian posterior distribution (*not* the minimum- χ^2) solution.

^fThe model magnitudes are available for the specific set of photometric bands included in the SED modeling, which differs from field to field.

Table 5. Column descriptions for the catalog presenting the galaxy physical properties computed from CIGALE

#	Parameter	Description
1	ID	Identification number
2	RA	Right ascension
3	DEC	Declination
4	photz	Photometric redshift used (from Table 2)
5	logM	Galaxy stellar mass [$\log M_{\odot}$]
6	logSFR	Instantaneous star-formation rate [$\log M_{\odot}/yr$]
7	logSFR100	100 Myr-averaged star-formation rate [$\log M_{\odot}/yr$]
8	Av	Dust attenuation (V-band) [mag]
9	logZsol	Stellar metallicity [$\log Z_{\odot}$]
10	logage	Age of the main stellar population [$\log yr$]
11	logtau	e-folding timescale of the main stellar population [$\log yr$]
12	f_burst	Fraction of mass formed in the late burst ^a
13	color_fuvnuv	Rest-frame FUV-NUV color
14	color_nuvr	Rest-frame NUV-R color
15	chi2	Reduced χ^2 value
16-	model_Fnu.*	Model template fluxes for observed photometric bands [μJy]

^aThe late burst is characterized as a (fixed) 10 Myr old exponentially declining episode of star-formation with an e-folding timescale of 50 Myr.

We thank the anonymous referee for their constructive feedback which helped improve the quality of the manuscript. The analysis presented in this paper is based on observations with the NASA/ESA Hubble Space Telescope obtained at the Space Telescope Science Institute, which is operated by the Association of Universities for Research in Astronomy, Incorporated, under NASA contract NAS5-26555. Support for Program Number HST-GO-15647 was provided through a grant from the STScI under NASA contract NAS5-26555. V.M., H.T., and X.W. acknowledge work carried out, in part, by IPAC at the California Institute of Technology, as was sponsored by the National Aeronautics and Space Administration.

Software: NumPy (Harris et al. 2020); SciPy (Virtanen et al. 2020); AstroPy (Astropy Collaboration et al. 2013, 2018, 2022); Matplotlib (Hunter 2007); FSPS (Conroy & Gunn 2010b); DENSE BASIS (Iyer et al. 2019); CIGALE (Boquien et al. 2019); EAZY (Brammer et al. 2008); BPZ (Benítez 2000; Benítez et al. 2004; Coe et al. 2006); LEPHARE (Arnouts et al. 1999; Ilbert et al. 2006); ZPHOT (Giallongo et al. 1998; Fontana et al. 2000)

REFERENCES

- Alavi, A., Siana, B., Richard, J., et al. 2014, ApJ, 780, 143, doi: [10.1088/0004-637X/780/2/143](https://doi.org/10.1088/0004-637X/780/2/143)
- . 2016, ApJ, 832, 56, doi: [10.3847/0004-637X/832/1/56](https://doi.org/10.3847/0004-637X/832/1/56)
- Arnouts, S., Cristiani, S., Moscardini, L., et al. 1999, MNRAS, 310, 540, doi: [10.1046/j.1365-8711.1999.02978.x](https://doi.org/10.1046/j.1365-8711.1999.02978.x)
- Ashby, M. L. N., Willner, S. P., Fazio, G. G., et al. 2013, ApJ, 769, 80, doi: [10.1088/0004-637X/769/1/80](https://doi.org/10.1088/0004-637X/769/1/80)
- . 2015, ApJS, 218, 33, doi: [10.1088/0067-0049/218/2/33](https://doi.org/10.1088/0067-0049/218/2/33)
- Astropy Collaboration, Robitaille, T. P., Tollerud, E. J., et al. 2013, A&A, 558, A33, doi: [10.1051/0004-6361/201322068](https://doi.org/10.1051/0004-6361/201322068)
- Astropy Collaboration, Price-Whelan, A. M., Sipőcz, B. M., et al. 2018, AJ, 156, 123, doi: [10.3847/1538-3881/aabc4f](https://doi.org/10.3847/1538-3881/aabc4f)
- Astropy Collaboration, Price-Whelan, A. M., Lim, P. L., et al. 2022, ApJ, 935, 167, doi: [10.3847/1538-4357/ac7c74](https://doi.org/10.3847/1538-4357/ac7c74)
- Baldry, I. K., Driver, S. P., Loveday, J., et al. 2012, MNRAS, 421, 621, doi: [10.1111/j.1365-2966.2012.20340.x](https://doi.org/10.1111/j.1365-2966.2012.20340.x)
- Balestra, I., Mainieri, V., Popesso, P., et al. 2010, A&A, 512, A12, doi: [10.1051/0004-6361/200913626](https://doi.org/10.1051/0004-6361/200913626)
- Barger, A. J., Cowie, L. L., & Wang, W. H. 2008, ApJ, 689, 687, doi: [10.1086/592735](https://doi.org/10.1086/592735)
- Barmby, P., Huang, J. S., Ashby, M. L. N., et al. 2008, ApJS, 177, 431, doi: [10.1086/588583](https://doi.org/10.1086/588583)
- Barro, G., Pérez-González, P. G., Cava, A., et al. 2019, ApJS, 243, 22, doi: [10.3847/1538-4365/ab23f2](https://doi.org/10.3847/1538-4365/ab23f2)
- Benítez, N. 2000, ApJ, 536, 571, doi: [10.1086/308947](https://doi.org/10.1086/308947)
- Benítez, N., Ford, H., Bouwens, R., et al. 2004, ApJS, 150, 1, doi: [10.1086/380120](https://doi.org/10.1086/380120)
- Bezanson, R., Wake, D. A., Brammer, G. B., et al. 2016, ApJ, 822, 30, doi: [10.3847/0004-637X/822/1/30](https://doi.org/10.3847/0004-637X/822/1/30)

- Bielby, R., Hudelot, P., McCracken, H. J., et al. 2012, *A&A*, 545, A23, doi: [10.1051/0004-6361/201118547](https://doi.org/10.1051/0004-6361/201118547)
- Blanton, M. R., & Roweis, S. 2007, *AJ*, 133, 734, doi: [10.1086/510127](https://doi.org/10.1086/510127)
- Boogaard, L. A., Brinchmann, J., Bouché, N., et al. 2018, *A&A*, 619, A27, doi: [10.1051/0004-6361/201833136](https://doi.org/10.1051/0004-6361/201833136)
- Boquien, M., Burgarella, D., Roehlly, Y., et al. 2019, *A&A*, 622, A103, doi: [10.1051/0004-6361/201834156](https://doi.org/10.1051/0004-6361/201834156)
- Bouwens, R. J., Illingworth, G. D., Oesch, P. A., et al. 2010, *ApJL*, 709, L133, doi: [10.1088/2041-8205/709/2/L133](https://doi.org/10.1088/2041-8205/709/2/L133)
- Brammer, G. B., van Dokkum, P. G., & Coppi, P. 2008, *ApJ*, 686, 1503, doi: [10.1086/591786](https://doi.org/10.1086/591786)
- Brammer, G. B., van Dokkum, P. G., Franx, M., et al. 2012, *ApJS*, 200, 13, doi: [10.1088/0067-0049/200/2/13](https://doi.org/10.1088/0067-0049/200/2/13)
- Bruzual, G., & Charlot, S. 2003, *MNRAS*, 344, 1000, doi: [10.1046/j.1365-8711.2003.06897.x](https://doi.org/10.1046/j.1365-8711.2003.06897.x)
- Burgarella, D., Buat, V., & Iglesias-Páramo, J. 2005, *MNRAS*, 360, 1413, doi: [10.1111/j.1365-2966.2005.09131.x](https://doi.org/10.1111/j.1365-2966.2005.09131.x)
- Byler, N., Dalcanton, J. J., Conroy, C., & Johnson, B. D. 2017, *ApJ*, 840, 44, doi: [10.3847/1538-4357/aa6c66](https://doi.org/10.3847/1538-4357/aa6c66)
- Calzetti, D., Armus, L., Bohlin, R. C., et al. 2000, *ApJ*, 533, 682, doi: [10.1086/308692](https://doi.org/10.1086/308692)
- Cardelli, J. A., Clayton, G. C., & Mathis, J. S. 1989, *ApJ*, 345, 245, doi: [10.1086/167900](https://doi.org/10.1086/167900)
- Chabrier, G. 2003, *PASP*, 115, 763, doi: [10.1086/376392](https://doi.org/10.1086/376392)
- Chabrier, G., Hennebelle, P., & Charlot, S. 2014, *ApJ*, 796, 75, doi: [10.1088/0004-637X/796/2/75](https://doi.org/10.1088/0004-637X/796/2/75)
- Coe, D., Benítez, N., Sánchez, S. F., et al. 2006, *AJ*, 132, 926, doi: [10.1086/505530](https://doi.org/10.1086/505530)
- Coil, A. L., Blanton, M. R., Burles, S. M., et al. 2011, *ApJ*, 741, 8, doi: [10.1088/0004-637X/741/1/8](https://doi.org/10.1088/0004-637X/741/1/8)
- Conroy, C., & Gunn, J. E. 2010a, *ApJ*, 712, 833, doi: [10.1088/0004-637X/712/2/833](https://doi.org/10.1088/0004-637X/712/2/833)
- . 2010b, *FSPS: Flexible Stellar Population Synthesis*, Astrophysics Source Code Library, record ascl:1010.043. <http://ascl.net/1010.043>
- Conroy, C., Gunn, J. E., & White, M. 2009, *ApJ*, 699, 486, doi: [10.1088/0004-637X/699/1/486](https://doi.org/10.1088/0004-637X/699/1/486)
- Cooper, M. C., Aird, J. A., Coil, A. L., et al. 2011, *ApJS*, 193, 14, doi: [10.1088/0067-0049/193/1/14](https://doi.org/10.1088/0067-0049/193/1/14)
- Cooper, M. C., Griffith, R. L., Newman, J. A., et al. 2012, *MNRAS*, 419, 3018, doi: [10.1111/j.1365-2966.2011.19938.x](https://doi.org/10.1111/j.1365-2966.2011.19938.x)
- Cristiani, S., Appenzeller, I., Arnouts, S., et al. 2000, *A&A*, 359, 489, doi: [10.48550/arXiv.astro-ph/0004213](https://doi.org/10.48550/arXiv.astro-ph/0004213)
- Croom, S. M., Smith, R. J., Boyle, B. J., et al. 2001, *MNRAS*, 322, L29, doi: [10.1046/j.1365-8711.2001.04474.x](https://doi.org/10.1046/j.1365-8711.2001.04474.x)
- Daddi, E., Cimatti, A., Renzini, A., et al. 2004, *ApJ*, 617, 746, doi: [10.1086/425569](https://doi.org/10.1086/425569)
- Dahlen, T., Mobasher, B., Faber, S. M., et al. 2013, *ApJ*, 775, 93, doi: [10.1088/0004-637X/775/2/93](https://doi.org/10.1088/0004-637X/775/2/93)
- Dale, D. A., Helou, G., Magdis, G. E., et al. 2014, *ApJ*, 784, 83, doi: [10.1088/0004-637X/784/1/83](https://doi.org/10.1088/0004-637X/784/1/83)
- Damjanov, I., Zahid, H. J., Geller, M. J., Fabricant, D. G., & Hwang, H. S. 2018, *ApJS*, 234, 21, doi: [10.3847/1538-4365/aaa01c](https://doi.org/10.3847/1538-4365/aaa01c)
- Davidzon, I., Ilbert, O., Laigle, C., et al. 2017, *A&A*, 605, A70, doi: [10.1051/0004-6361/201730419](https://doi.org/10.1051/0004-6361/201730419)
- Dickinson, M., Bergeron, J., Casertano, S., et al. 2003, *Great Observatories Origins Deep Survey (GOODS) Validation Observations*, Spitzer Proposal ID 196
- Doherty, M., Bunker, A. J., Ellis, R. S., & McCarthy, P. J. 2005, *MNRAS*, 361, 525, doi: [10.1111/j.1365-2966.2005.09191.x](https://doi.org/10.1111/j.1365-2966.2005.09191.x)
- Domínguez, A., Siana, B., Brooks, A. M., et al. 2015, *MNRAS*, 451, 839, doi: [10.1093/mnras/stv1001](https://doi.org/10.1093/mnras/stv1001)
- Draine, B. T., & Li, A. 2007, *ApJ*, 657, 810, doi: [10.1086/511055](https://doi.org/10.1086/511055)
- Emami, N., Siana, B., Weisz, D. R., et al. 2019, *ApJ*, 881, 71, doi: [10.3847/1538-4357/ab211a](https://doi.org/10.3847/1538-4357/ab211a)
- Fan, X., Strauss, M. A., Becker, R. H., et al. 2006, *AJ*, 132, 117, doi: [10.1086/504836](https://doi.org/10.1086/504836)
- Ferreras, I., Pasquali, A., Malhotra, S., et al. 2009, *ApJ*, 706, 158, doi: [10.1088/0004-637X/706/1/158](https://doi.org/10.1088/0004-637X/706/1/158)
- Fioc, M., & Rocca-Volmerange, B. 1997, *A&A*, 326, 950, doi: [10.48550/arXiv.astro-ph/9707017](https://doi.org/10.48550/arXiv.astro-ph/9707017)
- Fontana, A., D’Odorico, S., Poli, F., et al. 2000, *AJ*, 120, 2206, doi: [10.1086/316803](https://doi.org/10.1086/316803)
- Fontana, A., Dunlop, J. S., Paris, D., et al. 2014, *A&A*, 570, A11, doi: [10.1051/0004-6361/201423543](https://doi.org/10.1051/0004-6361/201423543)
- Giallongo, E., D’Odorico, S., Fontana, A., et al. 1998, *AJ*, 115, 2169, doi: [10.1086/300361](https://doi.org/10.1086/300361)
- Giavalisco, M., Ferguson, H. C., Koekemoer, A. M., et al. 2004, *ApJL*, 600, L93, doi: [10.1086/379232](https://doi.org/10.1086/379232)
- Grazian, A., Fontana, A., de Santis, C., et al. 2006, *A&A*, 449, 951, doi: [10.1051/0004-6361:20053979](https://doi.org/10.1051/0004-6361:20053979)
- Grazian, A., Giallongo, E., Paris, D., et al. 2017, *A&A*, 602, A18, doi: [10.1051/0004-6361/201730447](https://doi.org/10.1051/0004-6361/201730447)
- Grogin, N. A., Kocevski, D. D., Faber, S. M., et al. 2011, *ApJS*, 197, 35, doi: [10.1088/0067-0049/197/2/35](https://doi.org/10.1088/0067-0049/197/2/35)
- Guo, Y., Ferguson, H. C., Giavalisco, M., et al. 2013, *ApJS*, 207, 24, doi: [10.1088/0067-0049/207/2/24](https://doi.org/10.1088/0067-0049/207/2/24)
- Gwyn, S. D. J. 2012, *AJ*, 143, 38, doi: [10.1088/0004-6256/143/2/38](https://doi.org/10.1088/0004-6256/143/2/38)
- Harris, C. R., Millman, K. J., van der Walt, S. J., et al. 2020, *Nature*, 585, 357, doi: [10.1038/s41586-020-2649-2](https://doi.org/10.1038/s41586-020-2649-2)
- Hasinger, G., Capak, P., Salvato, M., et al. 2018, *ApJ*, 858, 77, doi: [10.3847/1538-4357/aabacf](https://doi.org/10.3847/1538-4357/aabacf)

- Hathi, N. P., Ferreras, I., Pasquali, A., et al. 2009, *ApJ*, 690, 1866, doi: [10.1088/0004-637X/690/2/1866](https://doi.org/10.1088/0004-637X/690/2/1866)
- Herenz, E. C., Urrutia, T., Wisotzki, L., et al. 2017, *A&A*, 606, A12, doi: [10.1051/0004-6361/201731055](https://doi.org/10.1051/0004-6361/201731055)
- Hildebrandt, H., Arnouts, S., Capak, P., et al. 2010, *A&A*, 523, A31, doi: [10.1051/0004-6361/201014885](https://doi.org/10.1051/0004-6361/201014885)
- Hopkins, A. M. 2018, *PASA*, 35, e039, doi: [10.1017/pasa.2018.29](https://doi.org/10.1017/pasa.2018.29)
- Hopkins, P. F., Kereš, D., Oñorbe, J., et al. 2014, *MNRAS*, 445, 581, doi: [10.1093/mnras/stu1738](https://doi.org/10.1093/mnras/stu1738)
- Hsu, L.-T., Lin, L., Dickinson, M., et al. 2019, *ApJ*, 871, 233, doi: [10.3847/1538-4357/aaf9a7](https://doi.org/10.3847/1538-4357/aaf9a7)
- Huang, J. S., Faber, S. M., Daddi, E., et al. 2009, *ApJ*, 700, 183, doi: [10.1088/0004-637X/700/1/183](https://doi.org/10.1088/0004-637X/700/1/183)
- Hunter, J. D. 2007, *Computing in Science & Engineering*, 9, 90, doi: [10.1109/MCSE.2007.55](https://doi.org/10.1109/MCSE.2007.55)
- Ilbert, O., Arnouts, S., McCracken, H. J., et al. 2006, *A&A*, 457, 841, doi: [10.1051/0004-6361:20065138](https://doi.org/10.1051/0004-6361:20065138)
- Ilbert, O., Capak, P., Salvato, M., et al. 2009, *ApJ*, 690, 1236, doi: [10.1088/0004-637X/690/2/1236](https://doi.org/10.1088/0004-637X/690/2/1236)
- Inami, H., Bacon, R., Brinchmann, J., et al. 2017, *A&A*, 608, A2, doi: [10.1051/0004-6361/201731195](https://doi.org/10.1051/0004-6361/201731195)
- Inoue, A. K. 2011, *MNRAS*, 415, 2920, doi: [10.1111/j.1365-2966.2011.18906.x](https://doi.org/10.1111/j.1365-2966.2011.18906.x)
- Iyer, K., & Gawiser, E. 2017, *ApJ*, 838, 127, doi: [10.3847/1538-4357/aa63f0](https://doi.org/10.3847/1538-4357/aa63f0)
- Iyer, K. G., Gawiser, E., Faber, S. M., et al. 2019, *ApJ*, 879, 116, doi: [10.3847/1538-4357/ab2052](https://doi.org/10.3847/1538-4357/ab2052)
- Jain, S., Tacchella, S., & Mosleh, M. 2024, *MNRAS*, 527, 3291, doi: [10.1093/mnras/stad3333](https://doi.org/10.1093/mnras/stad3333)
- Kajisawa, M., Ichikawa, T., Tanaka, I., et al. 2011, *PASJ*, 63, 379, doi: [10.1093/pasj/63.sp2.S379](https://doi.org/10.1093/pasj/63.sp2.S379)
- Kaushal, Y., Nersesian, A., Bezanson, R., et al. 2024, *ApJ*, 961, 118, doi: [10.3847/1538-4357/ad0c4e](https://doi.org/10.3847/1538-4357/ad0c4e)
- Kodra, D., Andrews, B. H., Newman, J. A., et al. 2023, *ApJ*, 942, 36, doi: [10.3847/1538-4357/ac9f12](https://doi.org/10.3847/1538-4357/ac9f12)
- Koekemoer, A. M., Faber, S. M., Ferguson, H. C., et al. 2011, *ApJS*, 197, 36, doi: [10.1088/0067-0049/197/2/36](https://doi.org/10.1088/0067-0049/197/2/36)
- Kriek, M., Shapley, A. E., Reddy, N. A., et al. 2015, *ApJS*, 218, 15, doi: [10.1088/0067-0049/218/2/15](https://doi.org/10.1088/0067-0049/218/2/15)
- Krogager, J. K., Zirm, A. W., Toft, S., Man, A., & Brammer, G. 2014, *ApJ*, 797, 17, doi: [10.1088/0004-637X/797/1/17](https://doi.org/10.1088/0004-637X/797/1/17)
- Kurczynski, P., Gawiser, E., Acquaviva, V., et al. 2016, *ApJL*, 820, L1, doi: [10.3847/2041-8205/820/1/L1](https://doi.org/10.3847/2041-8205/820/1/L1)
- Kurk, J., Cimatti, A., Daddi, E., et al. 2013, *A&A*, 549, A63, doi: [10.1051/0004-6361/201117847](https://doi.org/10.1051/0004-6361/201117847)
- Laidler, V. G., Papovich, C., Grogin, N. A., et al. 2007, *PASP*, 119, 1325, doi: [10.1086/523898](https://doi.org/10.1086/523898)
- Le Fèvre, O., Cassata, P., Cucciati, O., et al. 2013, *A&A*, 559, A14, doi: [10.1051/0004-6361/201322179](https://doi.org/10.1051/0004-6361/201322179)
- Le Fèvre, O., Tasca, L. A. M., Cassata, P., et al. 2015, *A&A*, 576, A79, doi: [10.1051/0004-6361/201423829](https://doi.org/10.1051/0004-6361/201423829)
- Leja, J., Carnall, A. C., Johnson, B. D., Conroy, C., & Speagle, J. S. 2019, *ApJ*, 876, 3, doi: [10.3847/1538-4357/ab133c](https://doi.org/10.3847/1538-4357/ab133c)
- Lilly, S. J., Le Fèvre, O., Renzini, A., et al. 2007, *ApJS*, 172, 70, doi: [10.1086/516589](https://doi.org/10.1086/516589)
- Lilly, S. J., Le Brun, V., Maier, C., et al. 2009, *ApJS*, 184, 218, doi: [10.1088/0067-0049/184/2/218](https://doi.org/10.1088/0067-0049/184/2/218)
- Lower, S., Narayanan, D., Leja, J., et al. 2020, *ApJ*, 904, 33, doi: [10.3847/1538-4357/abbfa7](https://doi.org/10.3847/1538-4357/abbfa7)
- Madau, P. 1995, *ApJ*, 441, 18, doi: [10.1086/175332](https://doi.org/10.1086/175332)
- Madau, P., & Dickinson, M. 2014, *ARA&A*, 52, 415, doi: [10.1146/annurev-astro-081811-125615](https://doi.org/10.1146/annurev-astro-081811-125615)
- Maraston, C. 2005, *MNRAS*, 362, 799, doi: [10.1111/j.1365-2966.2005.09270.x](https://doi.org/10.1111/j.1365-2966.2005.09270.x)
- Marchesini, D., van Dokkum, P. G., Förster Schreiber, N. M., et al. 2009, *ApJ*, 701, 1765, doi: [10.1088/0004-637X/701/2/1765](https://doi.org/10.1088/0004-637X/701/2/1765)
- Masters, D. C., Stern, D. K., Cohen, J. G., et al. 2019, *ApJ*, 877, 81, doi: [10.3847/1538-4357/ab184d](https://doi.org/10.3847/1538-4357/ab184d)
- McCracken, H. J., Milvang-Jensen, B., Dunlop, J., et al. 2012, *A&A*, 544, A156, doi: [10.1051/0004-6361/201219507](https://doi.org/10.1051/0004-6361/201219507)
- McLure, R. J., Pentericci, L., Cimatti, A., et al. 2018, *MNRAS*, 479, 25, doi: [10.1093/mnras/sty1213](https://doi.org/10.1093/mnras/sty1213)
- Mehta, V., Scarlata, C., Rafelski, M., et al. 2017, *ApJ*, 838, 29, doi: [10.3847/1538-4357/aa6259](https://doi.org/10.3847/1538-4357/aa6259)
- Mehta, V., Scarlata, C., Capak, P., et al. 2018, *ApJS*, 235, 36, doi: [10.3847/1538-4365/aab60c](https://doi.org/10.3847/1538-4365/aab60c)
- Mehta, V., Teplitz, H. I., Scarlata, C., et al. 2023, *ApJ*, 952, 133, doi: [10.3847/1538-4357/acd9cf](https://doi.org/10.3847/1538-4357/acd9cf)
- Meiksin, A. 2006, *MNRAS*, 365, 807, doi: [10.1111/j.1365-2966.2005.09756.x](https://doi.org/10.1111/j.1365-2966.2005.09756.x)
- Mérida, R. M., Pérez-González, P. G., Sánchez-Blázquez, P., et al. 2023, *ApJ*, 950, 125, doi: [10.3847/1538-4357/acc7a3](https://doi.org/10.3847/1538-4357/acc7a3)
- Mignoli, M., Cimatti, A., Zamorani, G., et al. 2005, *A&A*, 437, 883, doi: [10.1051/0004-6361:20042434](https://doi.org/10.1051/0004-6361:20042434)
- Momcheva, I. G., Brammer, G. B., van Dokkum, P. G., et al. 2016, *ApJS*, 225, 27, doi: [10.3847/0067-0049/225/2/27](https://doi.org/10.3847/0067-0049/225/2/27)
- Morishita, T., Abramson, L. E., Treu, T., et al. 2017, *ApJ*, 835, 254, doi: [10.3847/1538-4357/835/2/254](https://doi.org/10.3847/1538-4357/835/2/254)
- Moutard, T., Sawicki, M., Arnouts, S., et al. 2020, *MNRAS*, 494, 1894, doi: [10.1093/mnras/staa706](https://doi.org/10.1093/mnras/staa706)
- Muzzin, A., Marchesini, D., Stefanon, M., et al. 2013, *ApJ*, 777, 18, doi: [10.1088/0004-637X/777/1/18](https://doi.org/10.1088/0004-637X/777/1/18)

- Nayyeri, H., Hemmati, S., Mobasher, B., et al. 2017, *ApJS*, 228, 7, doi: [10.3847/1538-4365/228/1/7](https://doi.org/10.3847/1538-4365/228/1/7)
- Nedkova, K. V., Häußler, B., Marchesini, D., et al. 2021, *MNRAS*, 506, 928, doi: [10.1093/mnras/stab1744](https://doi.org/10.1093/mnras/stab1744)
- Nedkova, K. V., Rafelski, M., Teplitz, H. I., et al. 2024, arXiv e-prints, arXiv:2405.10908, doi: [10.48550/arXiv.2405.10908](https://doi.org/10.48550/arXiv.2405.10908)
- Newman, J. A., Cooper, M. C., Davis, M., et al. 2013, *ApJS*, 208, 5, doi: [10.1088/0067-0049/208/1/5](https://doi.org/10.1088/0067-0049/208/1/5)
- Noll, S., Burgarella, D., Giovannoli, E., et al. 2009, *A&A*, 507, 1793, doi: [10.1051/0004-6361/200912497](https://doi.org/10.1051/0004-6361/200912497)
- Nonino, M., Dickinson, M., Rosati, P., et al. 2009, *ApJS*, 183, 244, doi: [10.1088/0067-0049/183/2/244](https://doi.org/10.1088/0067-0049/183/2/244)
- Oke, J. B., & Gunn, J. E. 1983, *ApJ*, 266, 713, doi: [10.1086/160817](https://doi.org/10.1086/160817)
- Pacifici, C., Iyer, K. G., Mobasher, B., et al. 2023, *ApJ*, 944, 141, doi: [10.3847/1538-4357/acacff](https://doi.org/10.3847/1538-4357/acacff)
- Pasquali, A., Ferreras, I., Panagia, N., et al. 2006, *ApJ*, 636, 115, doi: [10.1086/497290](https://doi.org/10.1086/497290)
- Pentericci, L., McLure, R. J., Garilli, B., et al. 2018, *A&A*, 616, A174, doi: [10.1051/0004-6361/201833047](https://doi.org/10.1051/0004-6361/201833047)
- Picouet, V., Arnouts, S., Le Floch, E., et al. 2023, *A&A*, 675, A164, doi: [10.1051/0004-6361/202245756](https://doi.org/10.1051/0004-6361/202245756)
- Planck Collaboration, Ade, P. A. R., Aghanim, N., et al. 2016, *A&A*, 594, A13, doi: [10.1051/0004-6361/201525830](https://doi.org/10.1051/0004-6361/201525830)
- Prevot, M. L., Lequeux, J., Maurice, E., Prevot, L., & Rocca-Volmerange, B. 1984, *A&A*, 132, 389
- Rafelski, M., Wolfe, A. M., Cooke, J., et al. 2009, *ApJ*, 703, 2033, doi: [10.1088/0004-637X/703/2/2033](https://doi.org/10.1088/0004-637X/703/2/2033)
- Rafelski, M., Teplitz, H. I., Gardner, J. P., et al. 2015, *AJ*, 150, 31, doi: [10.1088/0004-6256/150/1/31](https://doi.org/10.1088/0004-6256/150/1/31)
- Ravikumar, C. D., Puech, M., Flores, H., et al. 2007, *A&A*, 465, 1099, doi: [10.1051/0004-6361:20065358](https://doi.org/10.1051/0004-6361:20065358)
- Retzlaff, J., Rosati, P., Dickinson, M., et al. 2010, *A&A*, 511, A50, doi: [10.1051/0004-6361/200912940](https://doi.org/10.1051/0004-6361/200912940)
- Riess, A. G., Strolger, L.-G., Casertano, S., et al. 2007, *ApJ*, 659, 98, doi: [10.1086/510378](https://doi.org/10.1086/510378)
- Roche, N. D., Dunlop, J., Caputi, K. I., et al. 2006, *MNRAS*, 370, 74, doi: [10.1111/j.1365-2966.2006.10439.x](https://doi.org/10.1111/j.1365-2966.2006.10439.x)
- Sanders, D. B., Salvato, M., Aussel, H., et al. 2007, *ApJS*, 172, 86, doi: [10.1086/517885](https://doi.org/10.1086/517885)
- Santini, P., Fontana, A., Grazian, A., et al. 2009, *A&A*, 504, 751, doi: [10.1051/0004-6361/200811434](https://doi.org/10.1051/0004-6361/200811434)
- Schlegel, D. J., Finkbeiner, D. P., & Davis, M. 1998, *ApJ*, 500, 525, doi: [10.1086/305772](https://doi.org/10.1086/305772)
- Scoville, N., Aussel, H., Brusa, M., et al. 2007, *ApJS*, 172, 1, doi: [10.1086/516585](https://doi.org/10.1086/516585)
- Shen, S., Mo, H. J., White, S. D. M., et al. 2003, *MNRAS*, 343, 978, doi: [10.1046/j.1365-8711.2003.06740.x](https://doi.org/10.1046/j.1365-8711.2003.06740.x)
- Silverman, J. D., Kashino, D., Sanders, D., et al. 2015, *ApJS*, 220, 12, doi: [10.1088/0067-0049/220/1/12](https://doi.org/10.1088/0067-0049/220/1/12)
- Skelton, R. E., Whitaker, K. E., Momcheva, I. G., et al. 2014, *ApJS*, 214, 24, doi: [10.1088/0067-0049/214/2/24](https://doi.org/10.1088/0067-0049/214/2/24)
- Speagle, J. S., Steinhardt, C. L., Capak, P. L., & Silverman, J. D. 2014, *ApJS*, 214, 15, doi: [10.1088/0067-0049/214/2/15](https://doi.org/10.1088/0067-0049/214/2/15)
- Stanford, S. A., Masters, D., Darvish, B., et al. 2021, *ApJS*, 256, 9, doi: [10.3847/1538-4365/ac0833](https://doi.org/10.3847/1538-4365/ac0833)
- Stefanon, M., Yan, H., Mobasher, B., et al. 2017, *ApJS*, 229, 32, doi: [10.3847/1538-4365/aa66cb](https://doi.org/10.3847/1538-4365/aa66cb)
- Straughn, A. N., Pirzkal, N., Meurer, G. R., et al. 2009, *AJ*, 138, 1022, doi: [10.1088/0004-6256/138/4/1022](https://doi.org/10.1088/0004-6256/138/4/1022)
- Strolger, L.-G., Riess, A. G., Dahlen, T., et al. 2004, *ApJ*, 613, 200, doi: [10.1086/422901](https://doi.org/10.1086/422901)
- Sun, G., Faucher-Giguère, C.-A., Hayward, C. C., et al. 2023a, *ApJL*, 955, L35, doi: [10.3847/2041-8213/acf85a](https://doi.org/10.3847/2041-8213/acf85a)
- Sun, L., Wang, X., Teplitz, H. I., et al. 2023b, arXiv e-prints, arXiv:2311.15664, doi: [10.48550/arXiv.2311.15664](https://doi.org/10.48550/arXiv.2311.15664)
- Taniguchi, Y., Scoville, N., Murayama, T., et al. 2007, *ApJS*, 172, 9, doi: [10.1086/516596](https://doi.org/10.1086/516596)
- Taniguchi, Y., Kajisawa, M., Kobayashi, M. A. R., et al. 2015, *PASJ*, 67, 104, doi: [10.1093/pasj/psv106](https://doi.org/10.1093/pasj/psv106)
- Teplitz, H. I., Rafelski, M., Kurczynski, P., et al. 2013, *AJ*, 146, 159, doi: [10.1088/0004-6256/146/6/159](https://doi.org/10.1088/0004-6256/146/6/159)
- Treister, E., Virani, S., Gawiser, E., et al. 2009, *ApJ*, 693, 1713, doi: [10.1088/0004-637X/693/2/1713](https://doi.org/10.1088/0004-637X/693/2/1713)
- Trump, J. R., Impey, C. D., Elvis, M., et al. 2009, *ApJ*, 696, 1195, doi: [10.1088/0004-637X/696/2/1195](https://doi.org/10.1088/0004-637X/696/2/1195)
- Trump, J. R., Weiner, B. J., Scarlata, C., et al. 2011, *ApJ*, 743, 144, doi: [10.1088/0004-637X/743/2/144](https://doi.org/10.1088/0004-637X/743/2/144)
- Trump, J. R., Konidaris, N. P., Barro, G., et al. 2013, *ApJL*, 763, L6, doi: [10.1088/2041-8205/763/1/L6](https://doi.org/10.1088/2041-8205/763/1/L6)
- Trump, J. R., Sun, M., Zeimann, G. R., et al. 2015, *ApJ*, 811, 26, doi: [10.1088/0004-637X/811/1/26](https://doi.org/10.1088/0004-637X/811/1/26)
- van der Wel, A., Franx, M., van Dokkum, P. G., et al. 2005, *ApJ*, 631, 145, doi: [10.1086/430464](https://doi.org/10.1086/430464)
- van der Wel, A., Noeske, K., Bezanson, R., et al. 2016, *ApJS*, 223, 29, doi: [10.3847/0067-0049/223/2/29](https://doi.org/10.3847/0067-0049/223/2/29)
- Vanzella, E., Cristiani, S., Dickinson, M., et al. 2008, *A&A*, 478, 83, doi: [10.1051/0004-6361:20078332](https://doi.org/10.1051/0004-6361:20078332)
- Vanzella, E., Giavalisco, M., Dickinson, M., et al. 2009, *ApJ*, 695, 1163, doi: [10.1088/0004-637X/695/2/1163](https://doi.org/10.1088/0004-637X/695/2/1163)
- Virtanen, P., Gommers, R., Oliphant, T. E., et al. 2020, *Nature Methods*, 17, 261, doi: [10.1038/s41592-019-0686-2](https://doi.org/10.1038/s41592-019-0686-2)
- Wang, X., Teplitz, H. I., Sun, L., et al. 2024, *Research Notes of the American Astronomical Society*, 8, 26, doi: [10.3847/2515-5172/ad1ff6](https://doi.org/10.3847/2515-5172/ad1ff6)

- Weaver, J. R., Davidzon, I., Toft, S., et al. 2023, *A&A*, 677, A184, doi: [10.1051/0004-6361/202245581](https://doi.org/10.1051/0004-6361/202245581)
- Weibel, A., Oesch, P. A., Barrufet, L., et al. 2024, arXiv e-prints, arXiv:2403.08872, doi: [10.48550/arXiv.2403.08872](https://doi.org/10.48550/arXiv.2403.08872)
- Weiner, B. 2009, Star formation, extinction and metallicity at $0.7 < z < 1.5$: H-alpha fluxes and sizes from a grism survey of GOODS-N, HST Proposal ID 11600. Cycle 17
- Weisz, D. R., Johnson, B. D., Johnson, L. C., et al. 2012, *ApJ*, 744, 44, doi: [10.1088/0004-637X/744/1/44](https://doi.org/10.1088/0004-637X/744/1/44)
- Whitaker, K. E., Labbé, I., van Dokkum, P. G., et al. 2011, *ApJ*, 735, 86, doi: [10.1088/0004-637X/735/2/86](https://doi.org/10.1088/0004-637X/735/2/86)
- Whitaker, K. E., Franx, M., Leja, J., et al. 2014, *ApJ*, 795, 104, doi: [10.1088/0004-637X/795/2/104](https://doi.org/10.1088/0004-637X/795/2/104)
- Windhorst, R. A., Cohen, S. H., Hathi, N. P., et al. 2011, *ApJS*, 193, 27, doi: [10.1088/0067-0049/193/2/27](https://doi.org/10.1088/0067-0049/193/2/27)
- Wirth, G. D., Trump, J. R., Barro, G., et al. 2015, *AJ*, 150, 153, doi: [10.1088/0004-6256/150/5/153](https://doi.org/10.1088/0004-6256/150/5/153)
- Wolf, C., Meisenheimer, K., Kleinheinrich, M., et al. 2004, *A&A*, 421, 913, doi: [10.1051/0004-6361:20040525](https://doi.org/10.1051/0004-6361:20040525)
- Wuyts, S., Labbé, I., Förster Schreiber, N. M., et al. 2008, *ApJ*, 682, 985, doi: [10.1086/588749](https://doi.org/10.1086/588749)
- Wuyts, S., van Dokkum, P. G., Franx, M., et al. 2009, *ApJ*, 706, 885, doi: [10.1088/0004-637X/706/1/885](https://doi.org/10.1088/0004-637X/706/1/885)
- Xue, Y. Q., Luo, B., Brandt, W. N., et al. 2016, *ApJS*, 224, 15, doi: [10.3847/0067-0049/224/2/15](https://doi.org/10.3847/0067-0049/224/2/15)
- Yoshikawa, T., Akiyama, M., Kajisawa, M., et al. 2010, *ApJ*, 718, 112, doi: [10.1088/0004-637X/718/1/112](https://doi.org/10.1088/0004-637X/718/1/112)